MASTERARBEIT | MASTER'S THESIS

Titel | Title

Tracing symbiont distribution in the holobiont: Investigating remote host tissues

verfasst von | submitted by

Alexandra Doskocilova

angestrebter akademischer Grad | in partial fulfilment of the requirements for the degree of

Master of Science (MSc)

Wien | Vienna, 2026

Studienkennzahl lt. Studienblatt	Degree programme code as it appears on the student record sheet:	UA 066 830
Studienrichtung lt. Studienblatt	Degree programme as it appears on the student record sheet:	Masterstudium Molecular Microbiology, Microbial Ecology and Immunobiology
Betreut von	Supervisor:	Univ.-Prof. Dr. Jillian Petersen

Acknowledgments

I would like to express my deepest gratitude to Dr. Cristina Alcaraz for her invaluable supervision, guidance, and continuous support throughout this thesis. Your expertise, patience, and encouragement have been fundamental to the completion of this work and to my growth as a researcher.

My sincere thanks also go to Assoc. Prof. Dr. Jillian Petersen for the opportunity to work within such an inspiring scientific environment, and for your insightful feedback and motivation that helped shape this project.

I am profoundly grateful to my parents for their unconditional love, encouragement, and unwavering belief in me. Thank you for always supporting my ambitions and giving me the strength to pursue my academic goals. I am equally thankful to my brothers, whose support, humour, and presence have been a constant source of motivation and balance throughout this journey.

The thesis underwent language and grammar improvement with Chat-GPT 5.1 and Grammarly AI tools, following the AI policy of the University of Vienna.

Abstract

Chemosynthetic bivalves of the family Lucinidae host intracellular sulphur-oxidising Gammaproteobacteria that fuel host nutrition in reduced marine sediments. These symbionts are traditionally assumed to be restricted to specialised gill bacteriocytes, yet recent work suggests that their distribution may extend into additional host tissue. This thesis examines five species: *Loripes orbiculatus*, *Loripinus fragilis*, *Phacoides pectinatus*, *Codakia orbicularis* (Lucinidae), and *Solemya velum* (Solemyidae), to assess whether multi-tissue symbiont presence is conserved across lineages and how transmission strategy influences anatomical localisation.

Using an integrative approach combining 16S rRNA gene sequencing, digital PCR targeting key sulphur-oxidation genes (*soxB*, *dsrC*, *svrhlE*), and fluorescence in situ hybridisation (FISH) with lineage-specific probes, I characterised symbiont presence across gill, foot, mantle, and visceral mass tissues. Across lucinids, all methods consistently identified the gills as the dominant symbiont niche, showing high symbiont abundance, strong functional gene signals, and dense intracellular localisation within bacteriocytes. Importantly, 16S sequencing and dPCR also revealed reproducible, low-to-moderate symbiont presence in foot, mantle, and visceral mass tissues in all lucinid species. FISH detection in these tissues was limited, likely due to low bacterial rRNA content, scarce cell distribution, and higher tissue autofluorescence.

Taken together, these findings demonstrate that the gills remain the central site of chemosynthetic symbiosis, however multi-tissue symbiont presence is a conserved but low-abundance feature across lucinids. Overall, this work challenges the long-standing assumption of strict gill confinement in Lucinidae and therefore provides new insight into the anatomical flexibility and evolutionary diversity of bivalve chemosymbioses.

Key words: Lucinidae, Solemyidae, sulphur-oxidising symbionts, chemoautotrophy, symbiont localisation, marine bivalves, host-microbe interactions

Zusammenfassung

Chemosynthetische Muscheln der Familie Lucinidae beherbergen intrazelluläre schwefeloxidierende Gammaproteobakterien, die die Ernährung des Wirts in nährstoffarmen Meeressedimenten unterstützen. Ursprünglich word angenommen, dass Symbioseinteraktion auf spezialisierte Kiemenbakteriozyten beschränkt ist. Doch neuere Arbeiten deuten darauf hin, dass die Symbionten möglicherweise auch in anderen Wirtsgeweben vorkommen können. In dieser Arbeit werden fünf Muschelrten untersucht: *Loripes orbiculatus, Loripinus fragilis, Phacoides pectinatus, Codakia orbicularis* (Lucinidae) und *Solemya velum* (Solemyidae), um zu beurteilen, ob das Vorkommen der Symbionten in verschiedene Geweben außerhalb der Kiemenbakteriozyten über verschiedene Abstammungslinien hinweg konserviert ist und wie die Übertragungsstrategie die anatomische Lokalisierung beeinflusst.

Mit einem integrativen Ansatz, der die Sequenzierung des 16S-rRNA-Gens, die digitale PCR auf wichtige Schwefeloxidationsgene (*soxB, dsrC, svrhlE*) und die Fluoreszenz-in-situ-Hybridisierung (FISH) mit stammspezifischen Sonden kombiniert, habe ich das Vorkommen von Symbionten in den Geweben der Kiemen, des Fußes, des Mantels und der viszeralen Masse charakterisiert. Bei allen Luciniden zeigten alle Methoden die Kiemen durchwegs als dominante Nische der Symbionten. Man findet eine hohe Symbiontenhäufigkeit, starke funktionelle Gensignale und dichte intrazelluläre Lokalisierung in den Bakteriozyten. Allerdings zeigten die 16S-Sequenzierung und dPCR auch eine immer wiederkehrende, geringe bis mäßige Präsenz von Symbionten in Fuß-, Mantel- und Viszeralgewebe aller Lucinidenarten. Das FISH-Signal in diesen Geweben war begrenzt, vermutlich aufgrund der geringen Präsenz an bakterieller rRNA, der geringen Zellzahl und der höheren Autofluoreszenz des Gewebes.

Zusammen zeigen diese Ergebnisse, dass zwar die Kiemen der zentrale Ort der chemosynthetischen Symbiose bleiben, das Vorkommen von Symbionten in anderen Geweben jedoch ein konserviertes Merkmal, wenn auch in geringeren Mengen, aller Lucinidae ist. Insgesamt stellt diese Arbeit die

langjährige Annahme einer strikten Beschränkung der Symbiose auf die Kiemen bei Lucinidae in Frage und liefert neue Erkenntnisse über die anatomische Flexibilität und evolutionäre Vielfalt der chemosynthetischen Symbiosen von Muscheln.

Schlüsselwörter: Lucinidae, Solemyidae, schwefeloxidierende Symbionten, Chemoautotrophie, Symbiontenlokalisierung, marine Muscheln, Wirt-Mikroben-Interaktionen

Abbreviations

ASV - Amplicon Sequence Variant

bp - Base Pair

DNA - Deoxyribonucleic Acid

dPCR - Digital Polymerase Chain Reaction

dsrC - Dissimilatory Sulphite Reductase Subunit C

EDTA - Ethylenediaminetetraacetic Acid

FISH - Fluorescence In Situ Hybridisation

H_2S - Hydrogen Sulphide

JMF - Joint Microbiome Facility

PCR - Polymerase Chain Reaction

PBS - Phosphate-Buffered Saline

PFA - Paraformaldehyde

RNA - Ribonucleic Acid

rRNA - Ribosomal RNA

svrhlE - *Solemya velum* RNA Helicase E

soxB - Sulphur Oxidation Enzyme B (thiosulphate oxidase)

TEM - Transmission Electron Microscopy

UV - Ultraviolet

V3-V4 - Hypervariable Regions 3 and 4 of the 16S rRNA Gene

µm - Micrometre

µL - Microlitre

1. Introduction

1. 1 Symbiosis as a Driver of Evolution and Ecology

Symbiosis, the persistent and often intimate interaction between phylogenetically distinct organisms, has long been recalled as a major driver of biological evolution (Moran, 2007). From the origins of eukaryotic cells through endosymbiosis to the formation of complex mutualisms such as mycorrhizal fungi and legume-rhizobia relationships, symbiotic partnerships highlight many of the most evolutionary transitions in the history of life (Pawlowska, 2024). In marine ecosystems, one of the most ecologically abundant forms of symbiosis is the cooperation between invertebrates and chemosynthetic bacteria (Dubilier et al., 2008). Chemosynthetic microorganisms are capable of obtaining energy from the oxidation of inorganic compounds, such as reduced sulphur species, to fix carbon dioxide into organic matter (Sogin et al., 2020).

These chemosynthetic symbioses are mainly important in environments where photosynthetic primary production is limited or absent. Examples include hydrothermal vents, cold seeps, oxygen minimum zones, and sulphidic sediments (Stewart et al., 2005). In these chemically reduced habitats, chemosynthetic bacteria act as the primary producers. They are supporting and maintaining a diverse array of animal hosts that would otherwise be unable to survive. These relationships allow the host to exploit niches that would be energetically inaccessible without microbial help (Stewart et al., 2005). Through the transfer of fixed carbon and essential nutrients from bacteria to their hosts, these symbioses have allowed diverse animal lineages to establish themselves in some of the most extreme environments on Earth (Xu et al., 2020).

1. 2 Lucinid Bivalves as a Model for Shallow-Water Chemosynthesis

Among the most widespread and ecologically influential examples of shallow-water chemosynthetic symbioses are those created by the bivalve family Lucinidae (Taylor and Glover, 2021). This family covers more than 400 described species and has a fossil record dating back to the Silurian period, approximately 340 million years ago (Stanley, 2014). The family Lucinidae represents one of the most diverse and globally distributed bivalve groups, occurring from tropical shallow waters to deep-sea environments. Within Lucinidae, this study focuses on representatives of three major subfamilies, each characterised by distinct evolutionary histories, host morphologies, and symbiont associations. Lucininae, Codakiinae, Pegophyseminae (Taylor et al., 2011). To place these taxa in a broader framework, Figure 1.1 shows a simplified phylogeny of family Lucinidae bivalves. Lucinidae form part of the Lucinoidea, a clade characterised by the evolution of intracellular sulphur-oxidising bacterial symbiosis. In contrast, the Solemyidae forms an early-branching lineage outside of the Lucinoidea (Figure 1.2). The two families display a fundamental distinction in symbiont transmission mode. Lucinidae acquire their symbionts horizontally from the environment each generation. Solemyidae transmit their symbionts vertically via the eggs, resulting in systemic distribution of symbionts throughout the host tissues (Krueger et al., 1996).

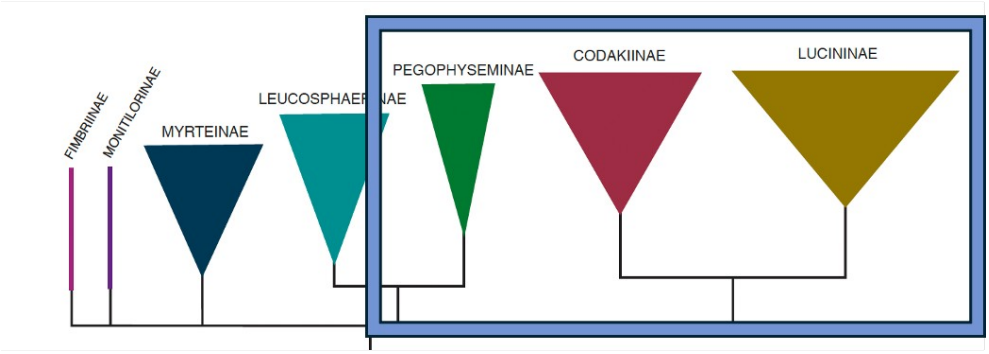

Figure 1. 1 Subfamilies of the family Lucinidae. A schematic representation of the major subfamilies within the family Lucinidae. Highlighted are the three subfamilies sampled in this study: Lucininae (*Loripes orbiculatus, Phacoides pectinatus*), Codakiinae (*Codakia orbicularis*), and Pegophyseminae (*Loripinus*

fragilis). These subfamilies span a broad range of evolutionary divergence within Lucinidae and cover species occupying different sedimentary habitats (Taylor et al., 2011).

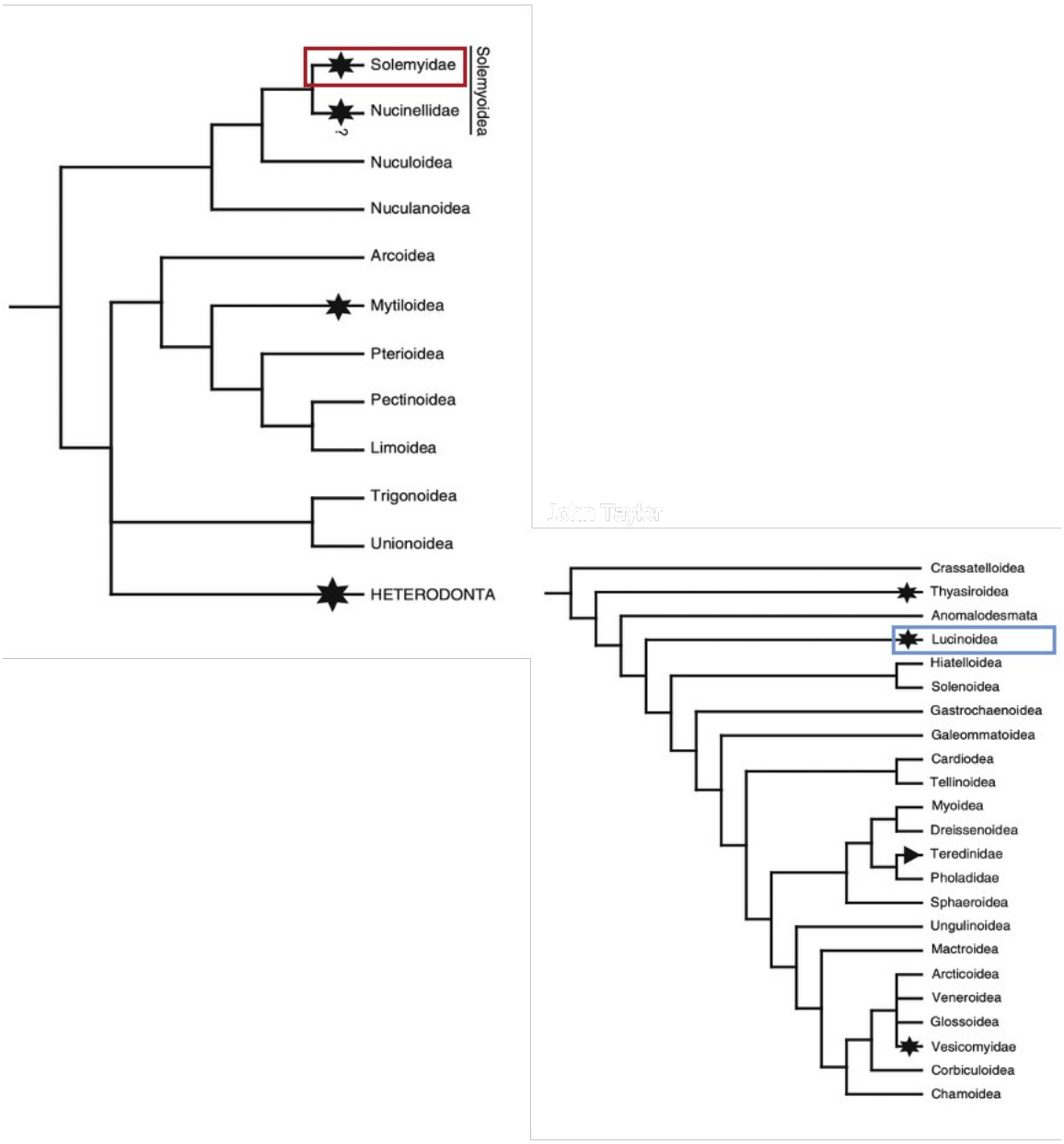

Figure 1. 2 Phylogenetic placement of Lucinidae and Solemyidae. A simplified phylogeny of bivalve superfamilies showing the position of Solemyidae as an early-branching lineage within the Solemyoidea, distinct from the Heterodonta clade. A phylogeny of Heterodonta bivalves (modified from Taylor and Glover, 2010) showing the placement of Lucinidae within Lucinoidea.

Loripes orbiculatus, *Phacoides pectinatus*, *Codakia orbicularis*, and *Loripinus fragilis* fall within Lucinidae, while *Solemya velum* (Solemyidae) is evolutionarily distant and included as an outgroup

to compare symbiont tissue localisation two distinct horizontal and vertical symbiont transmission pathways. Lucinid clams have established intracellular relationships with sulphur-oxidising Gammaproteobacteria, which allows them to prosper in coastal marine sediments where reduced sulphur compounds are abundant (Alcaraz et al., 2024). Unlike deep-sea chemosymbiotic bivalves, lucinids are found primarily in shallow and well-lit environments. They commonly inhabit silty and organic-rich sediments associated with seagrass meadows, mangroves, tidal lagoons, and estuaries. These habitats exhibit high microbial sulphate reduction rates, generating the hydrogen sulphide necessary to fuel the lucinid symbiosis (Duperron et al., 2013).

1. 3 Geological Distribution of Lucinid and Solemyid Species

The geological and ecological distribution of lucinid bivalves is remarkably broad and mirrors their adaptability to various sedimentary environments. *Loripes orbiculatus* is frequently found in Mediterranean and North Atlantic seagrass beds, especially in association with *Zostera* species (Rueda and Salas, 2008). *Phacoides pectinatus* and *Codakia orbicularis* are native to the Caribbean and Gulf of Mexico, typically thriving in mangrove-associated sediments and coastal lagoons (Martin et al., 2020; Tucker Abbott, 2001). *Loripinus fragilis* has a Mediterranean distribution (Taylor and Glover, 2005). *Solemya velum*, representing the closely related Solemyidae family, is included as an outgroup in this study. It is native to North Atlantic estuaries (Tucker Abbott, 2001) (Figure 1.3).

Figure 1. 3 Geographic distribution of bivalve species examined in this study.

Coloured points indicate sampling locations for each species: *Loripes orbiculatus* (Mediterranean, Piran in winter and summer; Rovinj in summer), *Loripinus fragilis* (Mediterranean, Rovinj), *Phacoides pectinatus* (Caribbean, Gulf of Mexico), *Codakia orbicularis* (Caribbean, Gulf of Mexico), and *Solemya velum* (Northwestern Atlantic, Rhode Island).

1. 4 Anatomy of Lucinid and Solemyid Clams

Bivalves have a laterally compressed body enclosed within two calcareous valves joined dorsally by a hinge ligament. The soft body is composed of several distinct parts, each with specific functions (Walker and Barnes, 1991). The gills (ctenidia) are large paired structures, which are the primary site of both respiration and filter feeding in most bivalves (Järnegren and Altin, 2006). In lucinids and solemyids, the gills also serve as specialised symbiont-housing organs. The cells, bacteriocytes, which can be found within the gill filaments possess intracellular sulphur-oxidising bacteria. These bacteria provide nutrition to the host via chemoautotrophy. The visceral mass houses the majority of the internal organs, including the digestive glands, gonads, stomach, and intestine (Alcaraz et al., 2024). The foot is a muscular, often protrusible organ, able to extend several lengths of the host body, used for burrowing into sediment and stabilising the animal's position. Additionally, the foot

is a crucial appendage because of its ability to construct mucus-lined tubes, necessary for accessing the overlying oxic seawater and providing the nutrients to the symbionts for chemosynthesis (Walker and Barnes, 1991). The mantle is a thin tissue layer that lines the inner surface of the shell and secretes calcium carbonate for shell growth. It encloses the mantle cavity, which houses the gills, foot, and siphons (Morton, 2024) (Figure 1. 4).

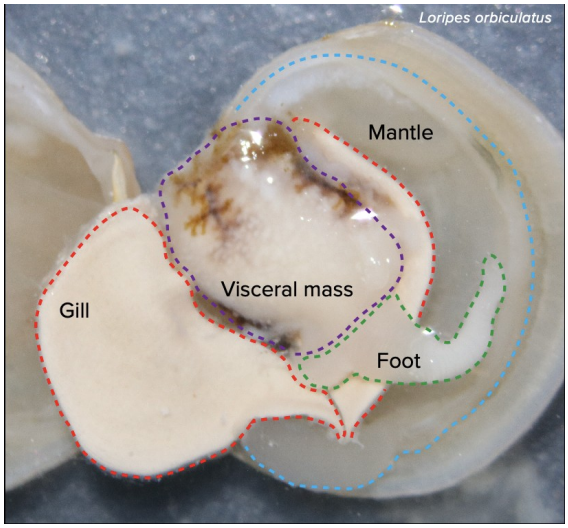

Figure 1. 4 Anatomy of *Loripes orbiculatus* with key tissues sampled for symbiont analyses

Schematic representation of *Loripes orbiculatus* illustrating major anatomical structures relevant to symbiosis research. The gill (ctenidium) is highlighted as the primary site of intracellular sulphur-oxidising symbionts housed within specialised bacteriocytes. The visceral mass, containing the digestive and reproductive organs, was sampled to assess potential background microbial presence and non-gill-associated symbiont signals. The mantle, forming the outer body wall and secreting the shell, and the muscular foot, used for burrowing and sediment interaction, were included to evaluate possible tissue-specific differences in microbial load and sediment-associated bacteria. Anatomical illustration adapted with permission from Cristina Alcaraz.

1. 5 Mutual Benefits of the Symbiotic Partnership

The mutualism between lucinid clams and their intracellular bacterial symbionts is a highly assimilated nutritional union. Symbionts are located within bacteriocytes, which are specialised host cells in the gill epithelium. In the bacteriocytes oxidation of reduced sulphur compounds (e.g.,

hydrogen sulphide and thiosulphate) to generate energy, takes place via the help of symbionts. The resulting compounds are used to fix inorganic carbon through the Calvin-Benson-Bassham cycle (Alcaraz et al., 2024). The resulting organic compounds are transferred to the host, often providing the clam's primary nutritional source (Petersen et al., 2016). In some invertebrate species, this dependence is so extreme that the digestive tract is reduced, indicating a shift from filter feeding to chemosynthetic nutrition, e.g *Riftia pachyptila* (Petersen and Yuen, 2021).

The host actively supports its symbionts by regulating behaviour and physiology to deliver both oxygen and sulphide to the gills (Figure 1. 5). Through burrowing, postural positioning, and vascularised gill structures, lucinids maintain access to both electron donors and acceptors (Chi-Ho Ip et al., 2020). This mutual exchange shows a mutualistic partnership benefiting both host and symbiont.

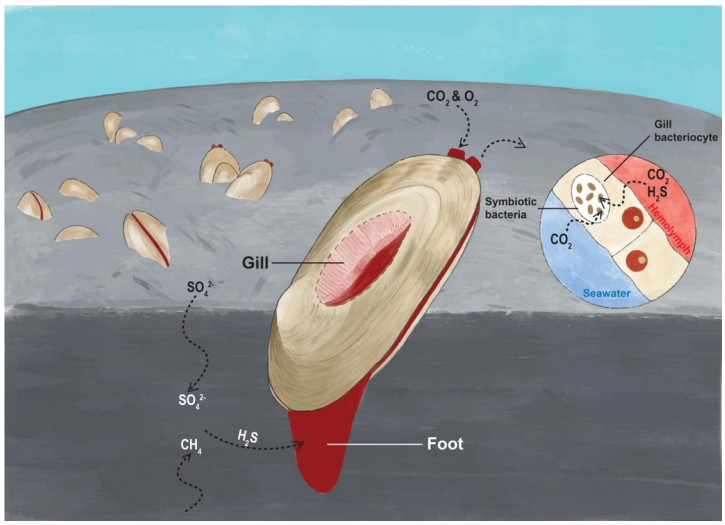

Figure 1. 5 Diagram of chemosynthetic symbiosis in a clam. Sulphur-oxidising bacteria are housed within specialised gill cells called bacteriocytes. The symbionts use hydrogen sulphide (H_2S) and oxygen (O_2) supplied by the clam to oxidise sulphur and fix inorganic carbon dioxide (CO_2) into organic carbon compounds. These fixed organic carbon products are then transferred to the host, providing it with a primary source of nutrition. Arrows indicate the flow of substrates and products between the environment, symbionts, and host (Chi-Ho Ip et al., 2020)

Sulphur-oxidising bacterial symbionts in lucinid and solemyid bivalves are members of the Gammaproteobacteria class. To detect, quantify, and functionally characterise these symbionts, several conserved marker genes are routinely targeted:

16S rRNA gene: A universally conserved component of the bacterial ribosome. Its conserved regions enable broad-range detection of bacteria, while its variable regions offer taxonomic discrimination. It is widely used to estimate total bacterial load and assess symbiont community composition in lucinid symbioses (Brissac et al., 2016).

***dsrC* gene**: Encodes a key component of the dissimilatory sulphite reductase complex. In sulphur-oxidising bacteria, *dsrC* functions in reverse compared to sulphate-reducing organisms, facilitating the oxidation of stored sulphur to sulphite, a central step in sulphur-based energy metabolism (Osvatic et al., 2023). Its presence indicates the symbiont's capacity for oxidative sulphur metabolism.

***soxB* gene**: Part of the Sox (sulphur oxidation) enzyme system, *soxB* encodes a periplasmic thiosulphate-oxidising hydrolase critical for converting thiosulphate to sulphate. This gene is essential for the functionality of the Sox multi-enzyme complex and is widespread across diverse sulphur-oxidising bacterial groups (Sudo et al., 2024).

***svrhlE* gene**: Specific for *Solemya velum*, encodes an RNA helicase strongly upregulated in thiotrophic symbionts during active sulphur oxidation and carbon fixation. Transcriptomic analyses of *S. velum* symbionts show that *svrhlE* expression increases in conditions promoting chemolithoautotrophy, linking it to symbiont metabolic activation and protein translation during sulphur oxidation (Russell et al., 2018).

Together, *16S rRNA*, *dsrC*, *soxB* represent complementary markers that enable detection (*16S*), metabolic potential assessment for sulphur oxidation (*dsrC*), and specific pathway identification (*soxB*), forming the molecular basis for characterising chemosynthetic symbioses in lucinids.

1. 6 Ecological Roles and Ecosystem Services

Beyond the individual benefits to the host, lucinid symbioses have extensive effects on benthic biogeochemistry (Reynolds et al., 2007). By actively oxidising toxic sulphide in sediments, lucinids detoxify porewaters. Presence of lucinids therefore promotes the health and productivity of nearby organisms, particularly seagrasses (Reynolds et al., 2007). These effects support a range of ecosystem services such as carbon sequestration, shoreline stabilisation, and the supply of essential nutrients for marine fauna (Chin et al., 2020). Their presence can crucially increase the resilience and efficiency of coastal marine ecosystems, which are progressively under threat from climate change, eutrophication, and habitat degradation (de Fouw et al., 2016).

1. 7 Knowledge Gaps: Symbiont Acquisition and Tissue Distribution

Despite decades of research into lucinid symbioses, many aspects of their developmental biology and symbiont dynamics remain unclear. Unlike *Solemya velum*, which inherits symbionts vertically via the egg cytoplasm, lucinids acquire symbionts horizontally from the surrounding environment (Gros et al., 2012). This mode of transmission indicates flexibility but also establishes vulnerability, as symbiont acquisition relies on the existence of compatible free-living bacteria and suitable environmental cues (Béziat et al., 2024). The timing, anatomical pathways, and molecular mechanisms of this acquisition remain poorly understood.

Moreover, the well-established pretence that symbionts are limited exclusively to the gill lamellae has recently been disputed. Alcaraz et al. (2024) used molecular and histological methods to show that in *Loripes orbiculatus*, sulphur-oxidising symbionts also colonise outside the gills. If such extensive colonisation is common among lucinids, it could be the evidence of internal microbial reservoirs, This is particularly important for maintaining symbiosis under environmental stress or following symbiont loss.

1. 8 Study Species and Comparative Framework

This thesis examines five bivalve species to determine whether multi-tissue colonisation by sulphur-oxidising symbionts is a conserved or lineage-specific trait. The main species include *Loripes orbiculatus*, *Phacoides pectinatus*, *Codakia orbicularis*, *Loripinus fragilis*, and *Solemya velum*. These species cover a broad phylogenetic and ecological spectrum within the family Lucinidae. By including species from different geological regions, habitat types, and symbiont transmission strategies, this study allows for comparative analysis of tissue-specific colonisation patterns and their evolutionary significance.

1. 9 Research Hypothesis and Objectives

The central hypothesis of this thesis is that tissue-wide colonisation by sulphur-oxidising symbionts is a phylogenetically conserved feature of the Lucinidae family, rather than being unique to *Loripes orbiculatus*. If true, this would propose that lucinid hosts sustain internal microbial reservoirs throughout multiple tissues, potentially providing recolonisation after environmental stress and strengthening holobiont robustness.

To test this, the study combines multiple methodological approaches:

- Fluorescence in situ hybridisation (FISH) to visualise and localise symbionts within tissues.
- Digital PCR (dPCR) to quantify symbiont abundance using sulphur metabolism markers (e.g., *dsrC, soxB, 16S, svrhlE*).
- *16S rRNA* gene sequencing to confirm symbiont identity

This multi-tissue, multi-species framework will allow evaluation of anatomical symbiont distribution and its correlation with phylogenetic lineage, habitat type, and host morphology.

1. 10 Broader Impacts and Significance

By expanding the scope of lucinid symbiosis research beyond the gills, this study aims to reconsider existing models of host-microbe interaction, moving towards a holobiont-wide perspective. Confirming extensive tissue colonisation would further challenge the canonical gill-centric view and provide new insights into the flexibility of chemosynthetic symbioses. Because of the ecological significance of lucinids in assisting seagrass productivity and stabilising marine sediments, understanding of symbiont persistence mechanisms is highly relevant. As climate change, pollution, and coastal development persist to endanger marine ecosystems, it is necessary to understand the adaptability of foundational symbioses like that of lucinids which is a crucial part of biodiversity conservation and coastal ecosystem management.

2. Materials and Methods

2. 1 Sample Collection and Dissection

Specimens of the aforementioned clam species were collected and immediately transferred to the laboratory. An exception to this protocol was *Phacoides pectinatus* (provided by Lukas Leibrecht), which was maintained under controlled aqua lab conditions and supplied with an algal food source (~ 5 months). *Solemaya velum* was shipped in 70% ethanol from the collected site (provided by Dr. Roxanne A. Beinart). Dissections were carried out under sterile conditions to isolate four distinct tissues: foot, gills, visceral mass, and mantle. Tissues were dissected and rinsed three times in filtered fresh seawater (FFSW), snap-frozen in liquid nitrogen, and stored at -20°C until further use.

Table 2. 1 Bivalve species used in this study

Species	Subfamily	Transmission	Habitat	Location	No. of samples
Phacoides pectinatus	Lucininae	Horizontal	Mangrove sediment	Caribbean, Gulf of Mexico Lat16.2857461, Lon -60.446951	3
Codakia orbicularis	Codakiinae	Horizontal	Shallow lagoons	Caribbean, Gulf of Mexico Lat 16.214407, Lon -61.535583	3
Loripes orbiculatus	Lucininae	Horizontal	Seagrass beds	Mediterranean, Piran - summer Lat 45.179562, Lon 13.602006	5
Loripes orbiculatus	Lucininae	Horizontal	Seagrass beds	Mediterranean, Rovinj - summer Lat 45.178506, Lon 13.595371	5
Loripinus fragilis	Pegophyseminae	Horizontal	Seagrass beds	Mediterranean Lat 45.178506, Lon 13.595371	4
Solemaya velum	Solemyinae (outgroup)	Vertical	Estuarine mudflats	Northwestern Atlantic (NA)	4

2. 2 DNA Extraction

DNA was extracted from clam tissues using three different commercial kits, selected according to species and sample characteristics, to ensure optimal yield and purity.

For *Codakia orbicularis*, and *Phacoides pectinatus*, DNA was extracted using the innuPREP DNA Mini Kit 2.0 (Analytik Jena) with minor modifications to accommodate variable tissue sizes. Samples were placed in sterile 1.5 or 2.0 mL tubes, and 400-1200 µL of Lysis Solution CBV with 30 µL of Proteinase K was added, depending on tissue consistency. Following brief vortexing, samples were incubated at 56°C for approximately two hours or until complete lysis was confirmed visually. Lysates were centrifuged at maximum speed for 3 minutes, and the supernatant was transferred to a fresh tube. To remove residual RNA, 1.5 µL of RNase A (10 mg/mL; Thermo Fisher Scientific) was added. DNA binding was achieved by adding 200 µL of Binding Solution SBS before loading the lysates onto spin columns. Columns were washed twice with 650 µL and once with 300 µL of Washing Solution MS, and DNA was eluted twice with 25 µL of pre-warmed EB. Samples were stored at 4-8°C for short-term use and at -20°C for long-term preservation.

Samples of *Loripinus fragilis* were processed using the QIAamp UCP DNA Micro Kit (Qiagen), optimised for small or potentially degraded samples. Samples were lysed in 180 µL of Buffer ATL with 20 µL of Proteinase K at 56°C with shaking until complete digestion (up to 3 hours). The lysate was mixed with 200 µL of Buffer AL and incubated at 70°C for 10 minutes, followed by the addition of 200 µL ethanol. The mixture was transferred to spin columns, washed sequentially with Buffers AW1 and AW2, and DNA was eluted in 50 µL of EB before storage at -20°C.

For *Solemya velum*, *Loripes orbiculatus* (Piran - summer), and *Loripes orbiculatus* (Rovinj - summer), DNA was extracted using the DNeasy Blood & Tissue Kit (Qiagen) according to the manufacturer's protocol for animal tissues. Samples were lysed in 180 µL of Buffer ATL with 20 µL of Proteinase K at 56°C for 1-3 hours, depending on tissue size. Following lysis, 200 µL of Buffer AL was added, and the mixture was incubated at 70°C for 10 minutes. Ethanol (200 µL) was then added, and the lysate was loaded onto spin columns. Columns were washed with 500 µL each of Buffer AW1 and AW2, and DNA was eluted in 50 µL of EB. All DNA extracts were stored at -20°C until further analysis.

2. 3 DNA Quantification

DNA concentration was quantified using a Qubit 4 fluorometer with the dsDNA HS Assay Kit (Thermo Fisher Scientific), and purity was assessed using a NanoDrop One spectrophotometer (Thermo Fisher Scientific). Samples with 260/280 ratios of ~1.8 and 260/230 ratios of ~2.0-2.2 were considered of acceptable purity. DNA concentrations exceeding the assay's optimal range were diluted with EB.

2. 4 Fixation and Dehydration of Specimens

Whole specimens of the aforementioned clam species were fixed in 4% paraformaldehyde (PFA) prepared fresh by diluting 16% stock PFA (ThermoFisher Scientific) with seawater in a 1:3 ratio. Fixation was performed overnight at 4°C in 5 mL of fixative per specimen. Post-fixation, samples were washed three times for 10 minutes each in 1x phosphate-buffered saline (PBS), followed by sequential dehydration in 30%, 50%, and 70% ethanol for 10 minutes each. Samples were stored in 70% ethanol at 4°C until further processing.

2. 5 Fluorescence in situ Hybridisation (FISH)

Sectioning of FISH samples was performed by the VBCF facility. Clam samples were fixed in 4% PFA, then stored in 70% ethanol until further processing. Embedding and sectioning were carried out to obtain 5 µm-thick sections

2. 5. 1 Buffers and Reagents for FISH

All buffers were prepared using analytical-grade reagents from Sigma-Aldrich, Merck, or Thermo Fisher Scientific, following protocols from Cold Spring Harbor (CSH) and the Marine Biological Laboratory (MBL). Reagents, buffer compositions, and probe list are listed in Table 2. 2 - 2. 10.

Table 2. 2 0.5M EDTA (160 mL)

Component	Quantity
EDTA (g)	37.20 g

ddH_2O (initial volume)	128 mL
NaOH pellets (for pH 8.0)	~48 pellets (approx.)
Final volume	160 mL
Sterilization	Autoclave

Note: Adjust pH after EDTA dissolves (precipitates may appear before reaching pH 8.0). Use NaOH pellets to increase pH. The final solution should turn clear at the correct pH.

Table 2. 3 5 M NaCl (200 mL)

Component	Quantity
NaCl (g)	58.4 g
ddH_2O (initial volume)	160 mL
Final volume	200 mL
Sterilization	Autoclave
Storage	Room Temperature

Table 2. 4 1M Tris-HCl (pH 7.0) (200 mL)

Component	Quantity
Tris base (g)	24.2 g
ddH_2O (initial volume)	160 mL
HCl (to pH 7.0)	As needed
Final volume	200 mL
Sterilization	Autoclave
Storage	Room Temperature

Table 2. 5 20% SDS Solution (50 mL)

Component	Quantity
SDS (powder)	10 g
ddH_2O (initial volume)	40 mL
ddH_2O (final adjustment)	Bring to 50 mL total
Heating	68°C with stirring
Sterilization	**Do not autoclave**
Storage	Room Temperature, stable for 6 months
Safety Note	SDS is **toxic** at RT—handle with gloves and avoid inhalation

Table 2. 6 Hybridisation Buffer 0% PFA (50mL)

Component	Quantity
5M NaCl	9 mL
1M Tris-HCl (pH 7.0)	1 mL
MilliQ H_2O	35 mL
Dextran sulfate	5 g
20% SDS	10 µL
Blocking Reagent	5 mL
Heat	40-60°C to dissolve dextran
Storage	Aliquots at -20°C

Table 2. 7 Hybridisation Buffer 35% PFA (50mL)

Component	Quantity
5M NaCl	9 mL
1M Tris-HCl (pH 7.0)	1 mL
MilliQ H_2O	22.45 mL
Formamide	17.5 mL
Dextran sulfate	5 g
20% SDS	20 µL
Blocking Reagent	5 mL
Heat	40-60°C to dissolve dextran
Storage	Aliquots at -20°C

Table 2. 8 Hybridisation Buffer 50% PFA (50mL)

Component	Quantity
5M NaCl	9 mL
1M Tris-HCl (pH 7.0)	1 mL
MilliQ H_2O	10 mL
Formamide	25 mL
Dextran sulfate	5 g
20% SDS	20 µL
Blocking Reagent	5 mL
Heat	40-60°C to dissolve dextran
Storage	Aliquots at -20°C

Table 2. 9 200 mL Wash Buffer 35%

Component	Quantity
5M NaCl	2.8 mL
1M Tris-HCl	4 mL

0.5M EDTA	2 mL
MilliQ H_2O	191 mL or adjust to volume
SDS (10%)	200 µL (add last)
Storage	Room Temperature (months)
Notes	SDS can be 100 µL of 20% as alternative

*Can be stored at RT for months,

Table 2. 10 FISH probes

Probe Name	Fluorophore	Sequence (5' → 3')	Target Group	Modification
EUB I, II, III	Cy5	GCT GCC TCC CGT AGG AGT, GCA GCC ACC CGT AGG TGT, GCT GCC ACC CGT AGG TGT	Universal Bacteria (EUB338 family)	*DOPE
Gamma42a	Cy5	GCC TTC CCA CAT CGT TT	Gammaproteobacteria	DOPE
Sym845	Cy3	TTA GCT GCG CCA CTA AAC CCT	Sulfur-oxidizing symbionts (e.g. lucinid symbionts)	DOPE
Sed642	Cy3	ACC ATA CTC TAG CCT GCC AG	*Phacoides pectinatus* symbionts	DOPE
SymAf576	Cy3	GAC TTG GCC GCC TAC GCA CG	*Loripinus fragilis* symbionts	DOPE
Svsym47	Cy3	CCC GAA GGT ATT TTC GCG TTC GAC TTG CAT	*Solemaya velum* symbionts	DOPE
Non-Eub	Cy3	ACT CCT ACG GGA GGC AGC	Competitor to EUB338-I	DOPE

* Double Labelling of Oligonucleotide Probes

2. 5. 2 FISH set up

Fluorescence in situ hybridisation (FISH) was performed following a modified protocol optimised for symbiont detection in tissue sections. To prepare the hybridisation chamber, Falcon tubes were filled with a KimWipe soaked in approximately 1 mL of the corresponding hybridisation buffer. These tubes were pre-warmed in an incubator set to 46°C. Tissue sections on microscope slides were circled with a hydrophobic barrier using a PAP pen to confine reagents to the target area.

A volume of approximately 20 µL of hybridisation buffer was applied to each tissue section, adjusted depending on the size of the area. Subsequently, fluorescently labeled oligonucleotide

probes specific to the symbionts were added directly to the hybridisation buffer droplets. Care was taken to keep the slides covered throughout this step to minimise evaporation and photobleaching. Slides were then placed in the pre-warmed hybridisation chambers and incubated at 46°C for three hours. After hybridisation, the slides were quickly dipped into a 50 mL Falcon tube containing room temperature wash buffer, followed by a 15-minute incubation in a second Falcon tube containing wash buffer preheated to 48°C. Following the wash steps, slides were briefly rinsed three times in ice-cold Milli-Q water and allowed to air dry in the dark. Once dry, approximately 20 µL of DAPI (1 µg/mL) was applied to each section, and the slides were incubated in the dark for 15 minutes. Excess DAPI was removed by rinsing the slides in ice-cold Milli-Q water. After a final drying step in the dark, ~8 µL of ProLong™ Glass Antifade Mountant was applied to each section, with 4 µL on the slide and 4 µL on the underside of the coverslip. Coverslips were cleaned with KimWipes before being carefully placed over the samples, and any excess mounting medium was gently removed with a KimWipe.

2. 6 Microscopy techniques

2. 6. 1 FISH microscopy - THUNDER

Whole-mount preparations were made from entire specimens of each host species, except for *Codakia orbicularis*, where the visceral mass was dissected and used. Samples prepared for FISH were hybridised with fluorophore-labelled oligonucleotide probes specifically targeting the 16S rRNA of the symbionts associated with each host species. Imaging was performed using a Leica THUNDER Imager, which provides high-resolution fluorescence images with real-time computational clearing to reduce out-of-focus background. Appropriate excitation and emission filter sets were used for each fluorophore, and images were taken at multiple magnifications to document the spatial distribution of symbionts within host tissues. Acquisition parameters (exposure time, laser intensity, and gain) were kept constant within each species-probe combination to ensure comparability.

2. 7 General molecular methods

To detect and quantify symbiont-specific genes across different tissues, conventional PCR and digital PCR (dPCR) were performed. Primer sequences targeting the *16S rRNA*, s*oxB*, *dsrC and svrhlE* genes were sourced from published literature and synthesised by Biomers.

2. 7. 1 Agarose gel electrophoresis

To visualise PCR amplicons, 2.5% agarose gels were prepared by dissolving 2.5 g of agarose (Biozym) in 100 mL of 1X TAE buffer. Gels were cast and loaded with 10 µL of PCR product mixed with 2 µL TriTrack DNA Loading Dye (6X) (Thermo Fisher Scientific). A 50 bp DNA ladder (Thermo Fisher Scientific)) was used to determine fragment size. Electrophoresis was carried out at 100 V for ~ 45 minutes, and bands were visualised under UV illumination using a GelDoc XR+ imaging system (Bio-Rad).

2. 7. 2 Polymerase chain reaction (PCR)

Table 2. 11 PCR Primer Sequences

Target Gene	Primer	Sequence (5'-3')	Amplicon Size
16S rRNA	341F	CCT ACG GGN GGC WGC AG	444 bp
16S rRNA	785R	GAC TAC HVG GGT ATC TAA TCC	
soxB	*soxB_F*	ACC GAT ACC CAT GCA CAA CTC A	113 bp
soxB	*soxB_R*	TTG AGC AGA TTA TCG CCC ACC A	
dsrC	*dsrC_F_web*	AGT GAA GAT GTG GCC AAG G	126 bp
dsrC	*dsrC*_R_web	ACG TTC GTTA GGC TGA TTG	
svrhlE	112F	GGA CGG GAT ATC ATG GGT GG	605 bp
svrhlE	717R	CAG CCA GGA GAG GAG TTC AC	

PCR reactions were prepared using DreamTaq Green PCR Master Mix (Thermo Fisher Scientific). A total reaction volume of 50 µL contained master mix, each of forward and reverse primer (10 µM), template DNA, and PCR-grade water. Thermal cycler conditions for each gene are listed in Table 2. 12.

Table 2. 12 Components for PCR reaction

Component	Volume per Reaction (µL)
DreamTaq Green PCR Master Mix (2×)	22
Forward Primer	1
Reverse Primer	1
Template DNA	1
Nuclease-free water (PCR-grade)	25
Total Volume	**50**

Table 2. 13 Standard PCR conditions

Step	Temperature	Duration
Initial Denaturation	95°C	3 minutes
Denaturation (×35)	95°C	30 seconds
Annealing (×35)	55°C	30 seconds
Extension (×35)	72°C	30 seconds
Final Extension	72°C	5 minutes
Hold	12°C	∞

For each host species, conventional PCR was performed to detect the presence of four target genes: the bacterial *16S rRNA* gene, the *soxB* gene (sulphur oxidation), the *dsrC* gene (dissimilatory sulphite reductase) and the *svrhlE* gene (*Solemaya velum* specific). These loci were selected as molecular markers to verify the presence of the sulphur-oxidising symbionts within the specimens. PCRs were conducted on DNA extracted from gill tissues, as these are the primary sites of symbiont localisation in lucinid and solemyid bivalves. The resulting amplicons served as a qualitative confirmation of target gene presence and were later used as reference controls for subsequent digital PCR (dPCR) assays. After amplification, products were visualised on a 1.5% agarose gel to verify the expected band sizes. Samples showing successful amplification were sent for Sanger sequencing to the Microsynth sequencing facility (Vienna, Austria) to confirm the identity of the amplicon. Sequence data were compared to reference sequences in public databases to verify the genes' presence in each species.

2. 8 Digital PCR (dPCR) for Symbiont Gene Quantification

Digital PCR assays were performed to quantify symbiont gene abundance across multiple tissue types, including foot, mantle, visceral mass, and gill, from all investigated lucinid bivalve species: *Loripes orbiculatus*, *Phacoides pectinatus*, *Codakia orbicularis*, *Loripinus fragilis*, and *Solemya velum*.

Table 2. 14 Components for dPCR reaction

Component	Volume per reaction (µl)
3× EvaGreen PCR Master Mix	4
Forward primer 10 µM	0.5
Reverse primer 10 µM	0.5
RNase-free water	5
Template DNA or cDNA	2
Total volume	**12**

Prior to loading, sample concentrations were normalised based on DNA quantification to ensure optimal template input and minimise variability between reactions. Reactions were loaded onto an 8.5k nanoplate (24-well format), with a carefully measured volume of 10 µl per well to prevent the formation of bubbles, which could interfere with droplet generation and signal detection. Thermal cycling was performed using a Qiagen digital PCR system, following the manufacturer's recommended protocol.

Table 2. 15 Standard dPCR conditions

Step	Duration	Temperature (°C)
Initial heat activation	5 minutes	95
Denaturation	30 seconds	95
Annealing	30 seconds	60
Elongation	30 seconds	72
Final cool-down	5 minutes	40

The thermal cycling protocol consisted of two stages. The first stage included 35 cycles of denaturation, annealing, and elongation steps. This was followed by a second stage of 5 additional cycles of the same steps to enhance amplification specificity and yield.

Fluorescent detection was carried out exclusively in the green channel using an exposure duration of 350 milliseconds and a gain setting of 3 to maximise signal-to-noise ratio. This setup ensured highly sensitive and reproducible quantification of symbiont gene copies across tissue types and species.

2. 9 16S rRNA Gene Sequencing

To characterise the microbial communities associated with different host tissues, high-throughput *16S rRNA* gene amplicon sequencing targeting the V3-V4 hypervariable region was performed. The objective was to identify and compare the microbiome present in four tissue types: gills, foot, mantle, and visceral mass of lucinid bivalve hosts.

DNA was extracted from each tissue type using established protocols and submitted for amplicon sequencing to the Joint Microbiome Facility (JMF) of the Medical University of Vienna and the University of Vienna (Project IDs: JMF-2508-03 and JMF-2504-07). Library preparation followed the standard two-step PCR workflow described by Pjevac et al. (2021). The V3-V4 hypervariable region of the *16S rRNA* gene was amplified using the universal primer pair 341F (CCTACGGGNGGCWGCAG) and 785R (GACTACHVGGGTATCTAATCC) (Klindworth et al., 2012). Barcoded sequencing libraries were generated using the TruSeq Nano DNA Kit (Illumina) and sequenced on an Illumina MiSeq platform (V3 chemistry, 600 cycles).

Raw sequencing data were processed using the FASTQ workflow in Illumina BaseSpace with default settings. Demultiplexing was performed using the *demultiplex* Python package (Laros JFJ, github.com/jfjlaros/demultiplex), allowing one mismatch for barcodes and two mismatches for linkers and primers. Amplicon sequence variants (ASVs) were inferred using DADA2 v1.30 (Callahan et al., 2016) following the recommended pipeline (Callahan et al., 2016b). Forward and reverse reads were trimmed to 230 nt, with maximum expected error thresholds of 4 and 6, respectively. Read pairs that could not be merged were concatenated to retain sequence information.

Taxonomic classification of ASV sequences was conducted in DADA2 using the SILVA SSU Ref NR99 database (release 138.1) with a confidence threshold of 0.5 (Quast et al., 2012; McLaren and Callahan, 2021). All downstream analyses were performed in R v4.3.2 using Bioconductor v3.16 packages, including SummarizedExperiment v1.32, SingleCellExperiment v1.24, TreeSummarizedExperiment v2.6 (Huang et al., 2020), as well as phyloseq v1.44 (McMurdie and Holmes, 2013), microbiome v1.22 (Github.io, 2025), and microViz v0.10.5 (Barnett et al., 2021). For both the V3-V4 and V4-V5 datasets, ASVs lacking taxonomic assignments or classified as eukaryotic sequences, mitochondria, or chloroplasts were removed. Potential laboratory contaminants were further identified using the R package decontam v0.20 (Davis et al., 2018), applying a prevalence threshold of 0.5 against extraction negative controls, and excluded from subsequent analyses.

3. Results

Distribution and abundance of sulphur-oxidising bacterial symbionts across different host tissues and species were assessed using a combination of molecular and microscopy-based approaches. Each specimen was dissected into gill, mantle, foot, and visceral mass, and these tissues were analysed separately to see possible spatial variation in symbiont occurrence. Quantitative and qualitative data were obtained through high-resolution *16S rRNA* amplicon sequencing, FISH microscopy using symbiont-specific probes and digital PCR (dPCR) targeting functional genes (*soxB*, *dsrC*, and *svrhlE* in *Solemya*). Together, these complementary methods enabled a comparison of microbial community composition, symbiont abundance, and tissue localisation patterns across six host species and three geographic regions.

3.1 DNA Extraction and Amplicon Sequencing

DNA extracted from all tissues yielded high-quality material suitable for sequencing and dPCR. Taxonomic assignment identified a small number of highly abundant bacterial ASVs characteristic of the sulphur-oxidising symbionts known to associate with lucinid and solemyid clams, alongside a broader set of lower-abundance taxa typically found in marine sediments.

Across all lucinid species, gill tissues consistently showed strong enrichment of Gammaproteobacteria corresponding to species-specific chemosynthetic symbionts. In contrast, foot, mantle, and visceral mass displayed more diverse bacterial assemblages, including *Spirochaeta, Endozoicomonas, Sedimenticola, Flavobacteriaceae*, and other sediment-associated taxa. In the solemyid *S. velum*, a single Gammaproteobacterial ASV was dominant across all examined tissues, consistent with systemic distribution of vertically transmitted symbionts.

Below, tissue-level results for each species are summarised in Figure 3.1.

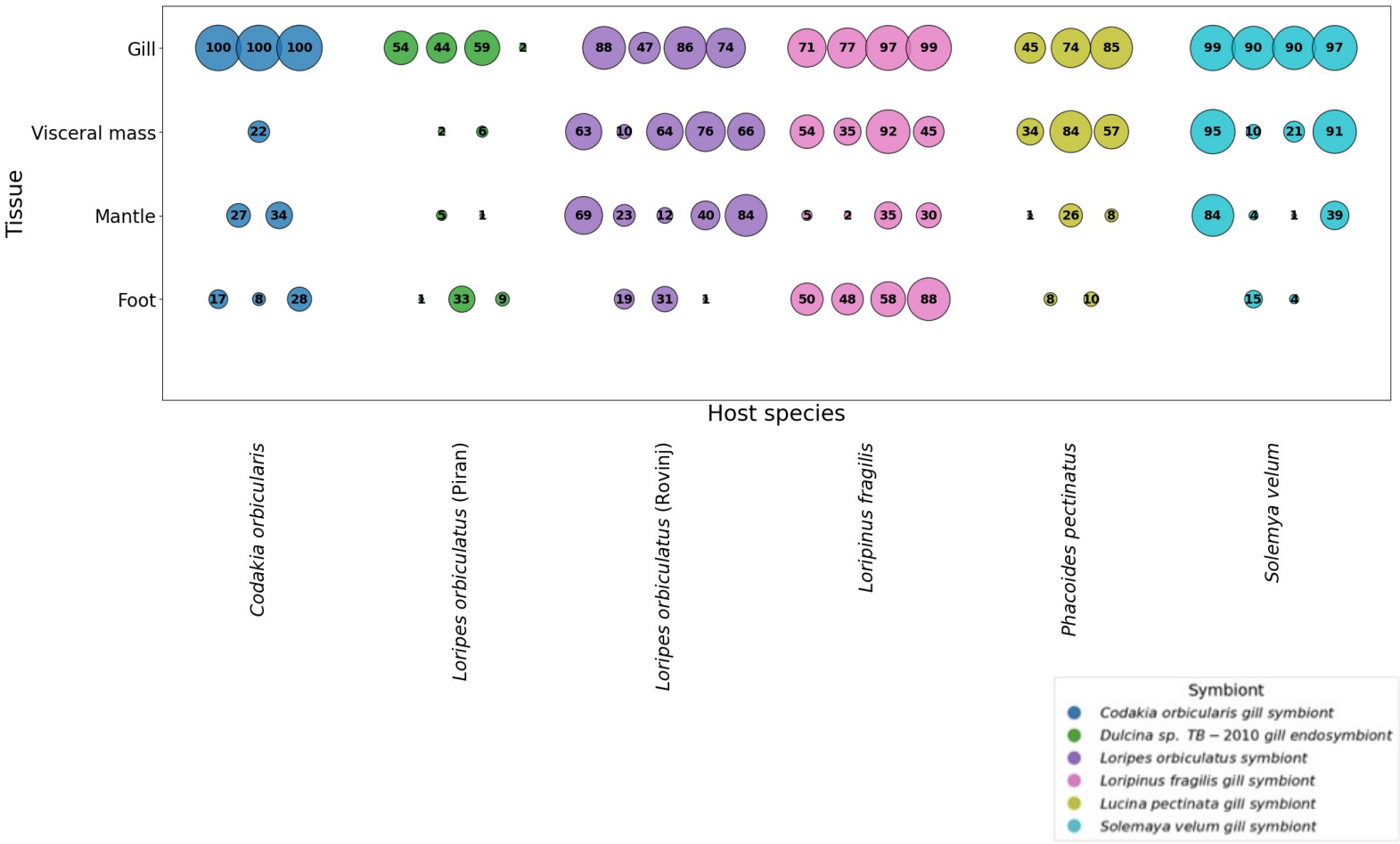

Figure 3. 1 Bubble plot illustrating the relative abundance and distribution of sulphur-oxidising symbiont ASVs across tissues and host species, based on simplified *16S rRNA* gene sequencing data. Each column represents one bivalve species or population (*Loripes orbiculatus* from Piran and Croatia, *Loripinus fragilis, Phacoides pectinatus, Codakia orbicularis*, and *Solemya velum*), and each row represents a host tissue (gill, visceral mass, mantle, foot). Circle size is proportional to the detected abundance of symbiont-associated ASVs in each tissue.

In *Loripes orbiculatus* from Piran, the bacterial community was dominated by ASVs belonging to *Ca.* Thiodiazotropha, with two highly abundant symbiont-associated lineages detected across tissues. The primary ASV corresponded to the *Dulcina sp.* TB-2010 gill endosymbiont, which ranged from 3-85% relative abundance depending on tissue type. A second *Ca.* Thiodiazotropha ASV occurred at lower but consistent levels, producing a combined symbiont-dominated signature (Figure 3. 1). As expected, symbiont abundance was highest in the gills (2-59% for the secondary

Dulcina ASV; 3-85% for the *Dulcina* ASV), clearly identifying the gill as the primary symbiont-harbouring organ. Non-gill tissues showed lower but detectable *Dulcina* gill symbiont signal: 9-33% in the foot, 1-5% in the mantle, and 2-6% in the visceral mass. Additional bacterial taxa occurred consistently at low abundance, with *Spirochaeta* forming the most prominent secondary component of the microbiome, while *Endozoicomonas* appeared primarily in the gills and *Cohaesibacter* and *Aliiroseovarius* were detected sporadically in the mantle (Figure S1).

The *Loripes orbiculatus* population from Rovinj exhibited a broadly comparable community composition but with a more heterogeneous distribution of *Ca.* Thiodiazotropha ASVs across tissues. The dominant symbiont corresponded to the *Loripes orbicularis* symbiont lineage, reaching 47-88% in the gills, 19-31% in the foot, 12-84% in the mantle, and 10-76% in the visceral mass. This population also harboured multiple additional *Ca.* Thiodiazotropha ASVs, including *Dulcina* sp. gill symbionts, *Loripes lucinalis* symbionts, and *Codakia costata* gill symbiont lineages, each contributing 1-17% relative abundance across samples, reflecting a richer symbiont strain diversity (six ASVs in total). As in Piran, *Shewanella* occurred in all tissues (occasionally up to 12%), while *Endozoicomonas* was found in the foot, visceral mass, and mantle, and members of the *Anaplasmataceae* appeared predominantly in the visceral mass (Figure S1).

In *Loripinus fragilis*, the microbial composition differed markedly from the two *Loripes* populations. The community was strongly dominated by a single ASV corresponding to the *Loripinus fragilis* gill symbiont lineage, which accounted for 71-99% of reads in gill tissue and remained abundant in non-gill tissues (48-88% in the foot, 35-95% in the visceral mass, and 2-35% in the mantle). *Spirochaeta* represented a consistent secondary taxon across all tissues (7-35%), while *Sedimenticola* appeared at low to moderate abundance. Thus, *Loripinus fragilis* exhibited the strongest whole-body dominance by a single symbiont lineage among the lucinids examined.

Phacoides pectinatus likewise displayed a symbiont-dominated microbiome, with ASVs assigned to the *Lucina pectinata* gill symbiont representing 45-85% of reads in the gill, 36-84% in the visceral

mass, 1-86% in the mantle, and 8-16%in the foot. Several sediment-associated taxa, including *Kistimonas*, *Brocadiaceae*, and *Sedimenticola,* occurred across tissues in low to moderate abundance, consistent with exposure to benthic microbial communities (Figure S2).

In *Codakia orbicularis*, *Ca.* Thiodiazotropha ASVs (*Codakia orbicularis* gill symbiont) represented nearly 100% of sequences in the gill, indicating a highly specific symbiont localisation. In non-gill tissues, however, symbiont abundance declined sharply (8-34%), and microbial diversity increased substantially, with frequent detection of *Spirochaeta*, *Cytophagales*, *Shimia*, *Mariniblastus*, *Dokdonia*, *Acidobacteria*, *Cohaesibacter*, and *Bythopirellula*. These patterns indicate the strongest gill restriction of any lucinid species in this study (Figure S2).

The solemyid *Solemya velum* showed a different microbiome structure consistent with vertical transmission. A single Gammaproteobacterial ASV corresponding to the canonical *S. velum* gill symbiont dominated all tissues, reaching 96-99% in the gill. The same lineage was present at measurable levels in the foot (4-84%), mantle (1-5%), and visceral mass (10-95%), reflecting systemic distribution of the vertically inherited symbiont.

Across lucinids, these results demonstrate a consistent pattern: gill tissues harbour the highest abundance of species-specific sulphur-oxidising symbionts, while non-gill tissues contain a combination of medium to low-level symbiont signal and diverse sediment-associated taxa. In contrast, *Solemaya velum* exhibits a vertically transmitted symbiont that dominates the microbiome of all tissues. Together, these amplicon sequencing data provide the quantitative foundation for interpreting tissue-specific symbiont distributions observed in the dPCR and FISH analyses.

3. 2 Digital PCR (dPCR) Quantification of Symbiont-Associated Genes

dPCR was used to quantify copy numbers of *soxB*, *dsrC*, and *svrhlE* across tissues. Gene copy numbers are expressed as $\log_{10}$ copies/gram of tissue. These genes serve as molecular markers

associated with sulphur oxidation (*soxB*), sulphur reduction (*dsrC*), and, in *Solemaya velum*, a symbiont-specific gene (*svrhlE*) enriched during chemoautotrophic metabolism.

Patterns were compared to 16S ASV abundance and to spatial symbiont localisation detected via FISH

3. 2. 1 *Loripes orbiculatus* (Piran population)

dPCR quantification of *dsrC* revealed a clear tissue-specific gradient, with the highest gene copy numbers in the gill, reaching approximately 10^8 copies/gram of tissue, followed by the visceral mass, which ranged between 10^6-10^7 copies/gram of tissue (Figure 3. 2. 1). The mantle contained fewer copies (10^4-10^7), and the foot exhibited the lowest abundance, consistently between 10^5-10^6 copies/gram of tissue. This distribution demonstrates a ~ 100-fold difference in *dsrC* abundance between gill and foot, and a ~10-fold difference between gill and mantle. The relatively elevated *dsrC* levels in the visceral mass indicate that this tissue contains a measurable amount of *dsrC*-bearing bacterial DNA, higher than the mantle and foot.

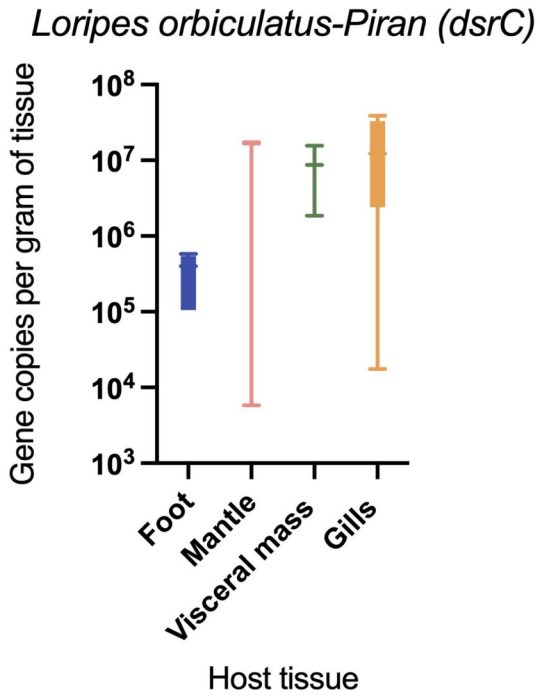

Figure 3. 2. 1. Tissue-specific quantification of *dsrC* gene copies in *Loripes orbiculatus* (Piran population). x-axis = host tissue, y- axis = $\log_{10}$ gene copies per gram of tissue. Highest copy numbers occur in gill and visceral mass (~10^7 copies/gram of tissue), with lower levels in foot and mantle.

3. 2. 2 *Loripes orbiculatus* (Rovinj population)

Quantification of *soxB* showed that the gene was detectable in all tissues, with maximum copy numbers in the gill and foot reaching 10^8-10^9 copies/gram of tissue (Figure 3.2.2). These values were consistently the highest among the four tissues. The visceral mass and mantle displayed lower levels, typically between 10^6-10^7 copies/gram of tissue. The dataset therefore exhibits a recurring pattern of gill = foot > visceral mass ~ mantle, with gill and foot showing approximately a tenfold increase over mantle.

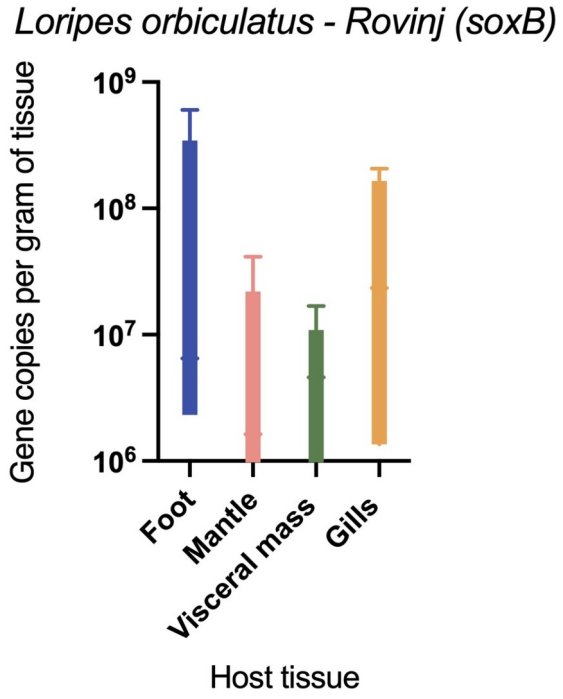

Figure 3. 2. 2. Tissue-specific quantification of *soxB* gene copies in *Loripes orbiculatus* (Rovinj population). x-axis = host tissue, y- axis = $\log_{10}$ gene copies per gram of tissue. Gill and foot tissues display the highest mean gene copy numbers (~10^8 copies/gram of tissue), whereas mantle and visceral mass contain lower but detectable levels (~10^6-10^7).

3. 2. 3 *Loripinus fragilis*

In *Loripinus fragilis*, *dsrC* was detected at very high copy numbers in both gill and foot, ranging from 10^9 to 10^{10} copies/gram of tissue (Figure 3. 2. 3). These values were an order of magnitude higher than those observed in *Loripes* species. The mantle and visceral mass displayed intermediate concentrations (10^7-10^9 copies/gram of tissue), which are slightly below than the gill and foot but remain well above detection threshold. The contrast between gill/foot and mantle/visceral mass is pronounced: gill and foot exhibit *dsrC* levels 10-1,000× higher than the mantle. Replicate variance was minimal, showing highly consistent *dsrC* detection across biological replicates.

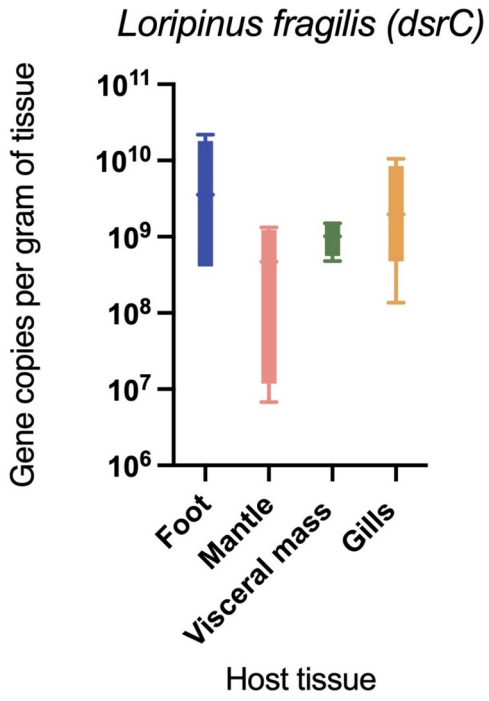

Figure 3. 2. 3. Digital PCR quantification of *dsrC* gene copies across tissues of *Loripinus fragilis*. x-axis = host tissue, y- axis = $\log_{10}$ gene copies per gram of tissue. Gill and foot samples display the highest *dsrC* abundance (10^9-10^{10} copies/gram of tissue).

3. 2. 4 *Phacoides pectinatus*

In *Phacoides pectinatus*, *dsrC* copy numbers were highest in the foot, reaching ~10^8 copies/gram of tissue, followed by visceral mass, which showed values between 10^6-10^7 and the gill (10^2-10^7) (Figure 3. 2. 4). The mantle contained marginally lower levels (<10^6 copies/gram of tissue). The distribution (foot > visceral mass > gill > mantle) demonstrates a strong concentration of *dsrC* across aforementioned tissues, with foot showing the highest mean abundance across replicates.

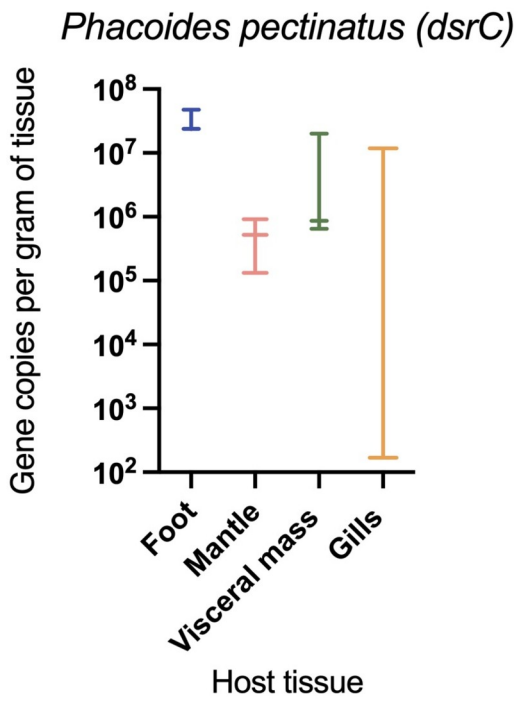

Figure 3. 2. 4. Quantification of *dsrC* gene copies across tissues of *Phacoides pectinatus*. x-axis = host tissue, y- axis = $\log_{10}$ gene copies per gram of tissue. Foot, visceral mass and gills display elevated *dsrC* abundance (~10^6-10^7 copies/gram of tissue), while mantle contain lower levels.

3. 2. 5 *Codakia orbicularis*

For *Codakia orbicularis*, *soxB* gene copy numbers were highest in the foot, reaching approximately 10^7 copies/gram of tissue, with comparable levels detected in the mantle and gill and visceral mass, around 10^7 copies/gram of tissue (Figure 3. 2. 5).

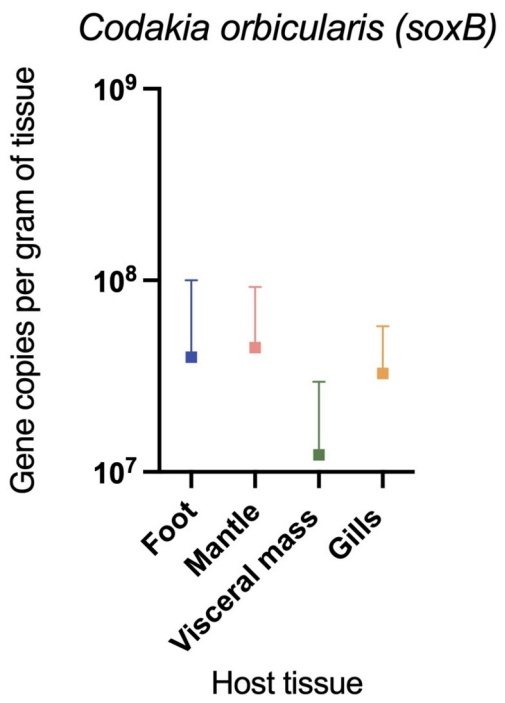

Figure 3. 2. 5. Quantification of *soxB* gene copies in *Codakia orbicularis* tissues. x-axis = host tissue, y-axis = $\log_{10}$ gene copies per gram of tissue. Foot tissue shows the highest *soxB* abundance (~10^5 copies/ gram of tissue), followed by mantle and gill (~10^4 copies/gram of tissue).

3. 2. 6 *Solemya velum*

In *Solemaya velum*, *svrhlE* gene copy numbers were consistently high across all tissues, ranging from 10^5-10^7 copies/gram of tissue (Figure 3. 2. 6). Among these, the gill exhibited the highest mean abundance, followed by the mantle and visceral mass. The foot showed slightly lower levels but remained within the same order of magnitude. The low replicate variance across all four tissues indicates a stable and uniform distribution of the *svrhlE* gene within the organism. The absence of large inter-tissue differences contrasts with the lucinids and reflects the systemic distribution of the dominant symbiont.

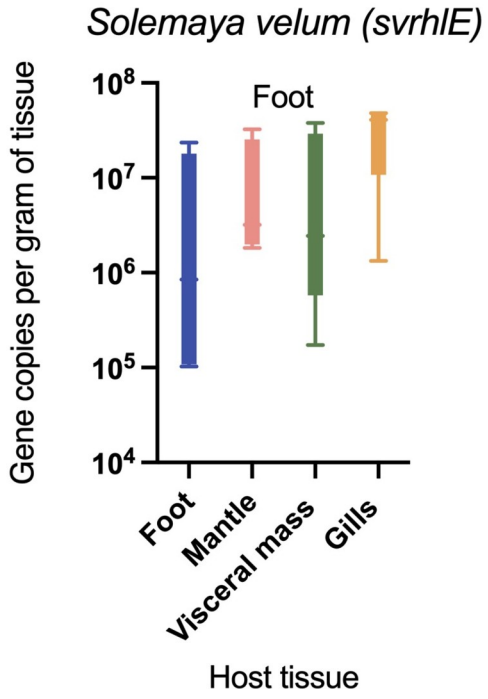

Figure 3. 2. 6. Quantification of *svrhlE* gene copy numbers in *Solemya velum* tissues.

x-axis = host tissue, y- axis = $\log_{10}$ gene copies per gram of tissue. Digital PCR results show that the values are approximately equal between different tissues.

3. 3 Fluorescence In Situ Hybridisation (FISH) Visualisation of Symbionts

Fluorescence in situ hybridisation (FISH) was performed on whole-body and dissected tissue preparations from six lucinid specimen and the solemyid *Solemya velum* to directly visualise the spatial distribution of intracellular symbiotic bacteria across different host tissues. Symbiont detection was achieved using lineage-specific 16S rRNA probes (Sym845 for *Ca.* Thiodiazotropha; SymAf576 for the *Loripinus fragilis* symbiont; Sed642 for the *Phacoides pectinatus* symbiont; and Svsym47 for the *Solemaya velum* symbiont). Probes carried a Cy3 fluorophore, while DAPI counterstaining enabled identification of host nuclei.

To confirm that all observed FISH signals reflected genuine probe hybridisation rather than autofluorescence or nonspecific binding, a full set of NON-EUB control images was examined for all species Supplementary Figure 3. These negative controls showed only diffuse background fluorescence and no probe-like signal. This indicates that the strong signals detected with symbiont-

specific probes in gill tissues, and the weaker but consistent signals in certain non-gill tissues, represent true symbiont.

3. 3. 1 *Loripes orbiculatus* (Piran population)

Hybridisation with the Sym845 probe resulted in intense and spatially coherent Cy3 fluorescence throughout the gill lamellae (Figure 3. 3. 1A-C). Fluorescently-labelled bacteria were clearly confined to host bacteriocytes, forming dense intracellular clusters consistent with canonical lucinid symbiont morphology. Cy3 signal consistently overlapped with DAPI, confirming localisation within host cells.

In addition to the gills, distinct but lower-intensity symbiont fluorescence was detected in the foot epithelium (Figure 3. 3. 1D). At high magnification, individual or small aggregates of bacterial cells hybridised with Sym845 were visible along epithelial folds. The distribution was patchy, but the signal appeared in all biological replicates (Figure 3. 3. 1E-G). This indicates that the presence of Sym845-positive bacteria in the foot is a reproducible feature of this population and not an artefact.

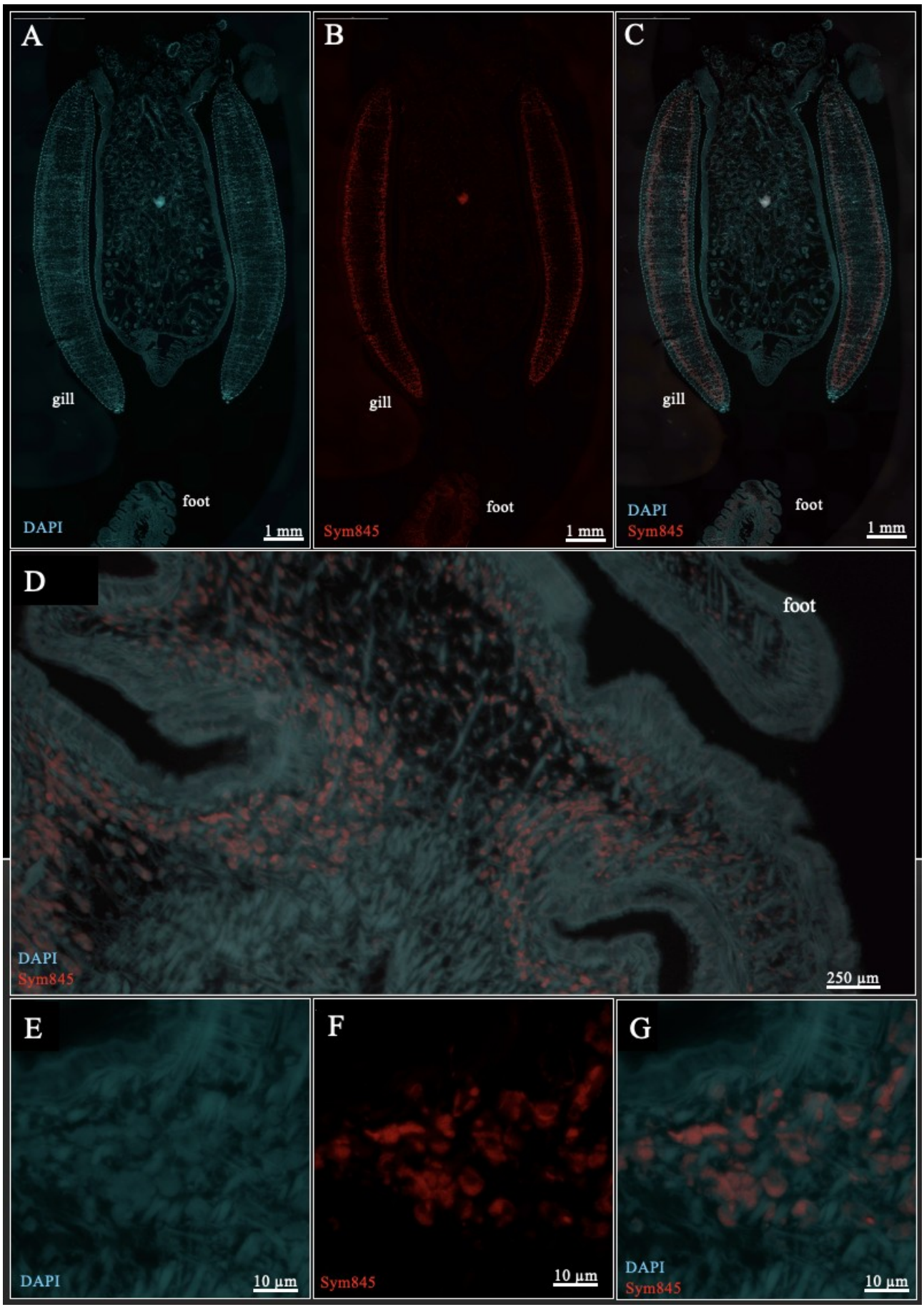
A
gill
foot
DAPI
1 mm
B
gill
foot
Sym845
1 mm
C
gill
foot
DAPI
Sym845
1 mm
D
foot
DAPI
Sym845
250 µm
E
DAPI
10 µm
F
Sym845
10 µm
G
DAPI
Sym845
10 µm

Figure 3. 3. 1. Localisation of bacterial symbionts in *Loripes orbiculatus* (Piran population). (A-C) Whole-body FISH image hybridised with the symbiont probe Sym845, stained with DAPI shows red fluorescence concentrated in gill regions. (D) Magnified view of the foot tissue (250 µm) showing distinct red fluorescence overlapping with DAPI-stained host nuclei (blue). (E-G) Higher magnification (10 µm) of foot epithelium showing DAPI (E), Sym845 (F), and merged channels (G), with clear red signal confirming the presence of bacterial cells.
Scale bars: A = 1 mm; B = 250 µm; C = 10 µm.

3. 3. 2 *Loripes orbiculatus* (Rovinj population)

In the Rovinj population, hybridisation with Sym845 again produced high-intensity fluorescence in gill bacteriocytes (Figure 3. 3. 2A-C). The signal followed the lamellar organisation of the gill, forming a continuous band of intracellular bacterial clusters occupying the entire bacteriocyte layer. Moderate Sym845 fluorescence was also detected in the foot (Figure 3. 3. 2D-I), where bacterial cells were identifiable based on size, shape, and characteristic probe signal. The consistency of the foot signal across magnifications and replicates indicates the presence of a stable, low-density symbiont population in this tissue.

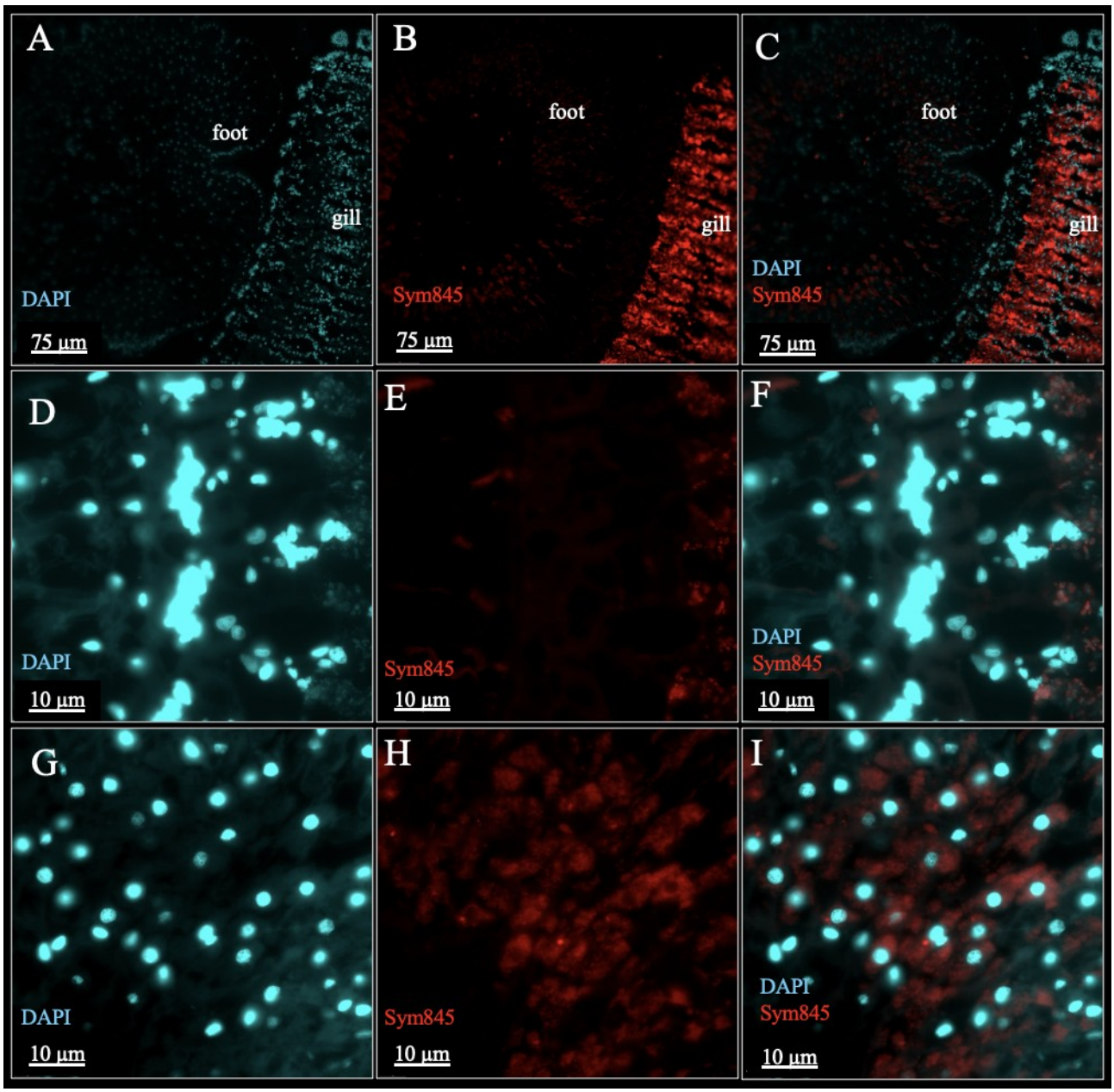

Figure 3. 3. 2. Tissue-specific distribution of bacterial signal in *Loripes orbiculatus* (Rovinj population). (A-C) FISH micrograph of gill tissue hybridised with Sym845 probe (red), showing dense fluorescence within bacteriocytes. (D-F) Moderate red fluorescence in the foot with DAPI (blue), Sym845, and merged channels. (G-I) Additional viewpoint of foot region showing bacterial morphology consistent with symbiont-like cells.

Scale bars: A-C =75 µm; D-I = 10 µm.

3. 3. 3 *Loripinus fragilis*

Hybridisation with the SymAf576 probe (Sudo et al., 2024) produced intense, well-defined Cy3 fluorescence exclusive to the gill bacteriocytes (Figure 3. 3. 3A-D). No signal was observed in foot, mantle, or visceral mass. Symbiont signal appeared as compact intracellular clusters within bacteriocytes, consistent with a dense symbiont population.

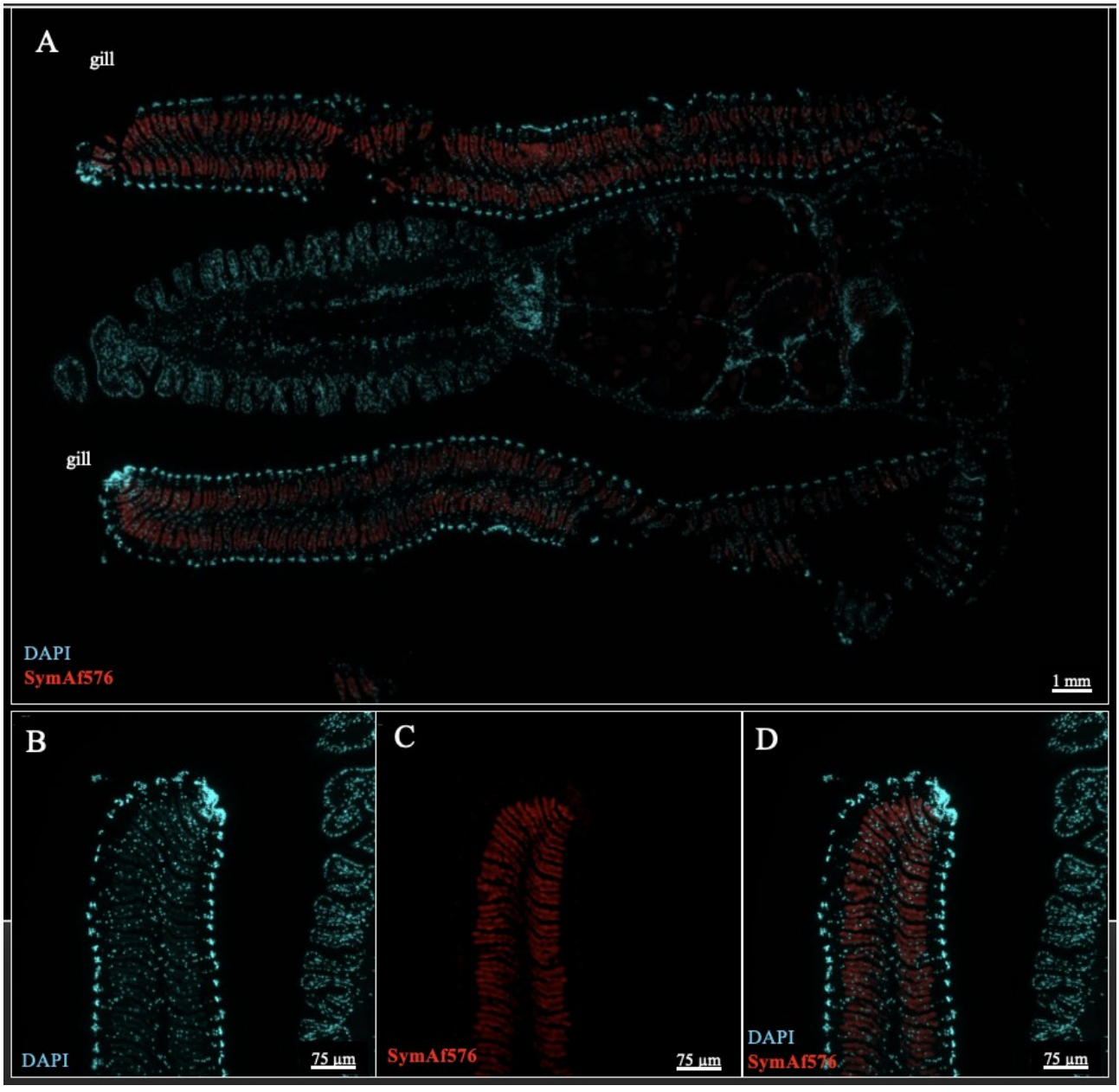

Figure 3. 3. 3. Detection of sulphur-oxidising symbionts in *Loripinus fragilis* gills using the SymAf576 probe. (A) Whole-body FISH image hybridised with the symbiont probe SymAf576, stained with DAPI shows red fluorescence concentrated in gill regions. (B-D) FISH image showing bright red fluorescence confined to bacteriocyte-rich areas of gill lamellae. Separate channels for DAPI, SymAf576, merged.

Scale bars: (A) = 1 mm; (B-D) = 75 µm

3. 3. 4 *Phacoides pectinatus*

Hybridisation with the Sed642 species-specific probe yielded strong red fluorescence in gill bacteriocytes, where symbiont cells densely packed the location (Figure 3. 3. 4 A-C). The distribution of signal mirrored the structural arrangement of bacteriocyte-rich lamellae, indicating abundant intracellular symbionts.

In addition to gill fluorescence, clear Sed642 signal was detected in the visceral mass (Figure 3. 3. 4D-F), where scattered bacterial cells or small clusters were visible among digestive epithelia. High-magnification imaging (Figure 3. 3. 4G-I) confirmed the presence of symbiont-sized, probe-positive cells in the visceral mass of *Phacoides pectinatus*.

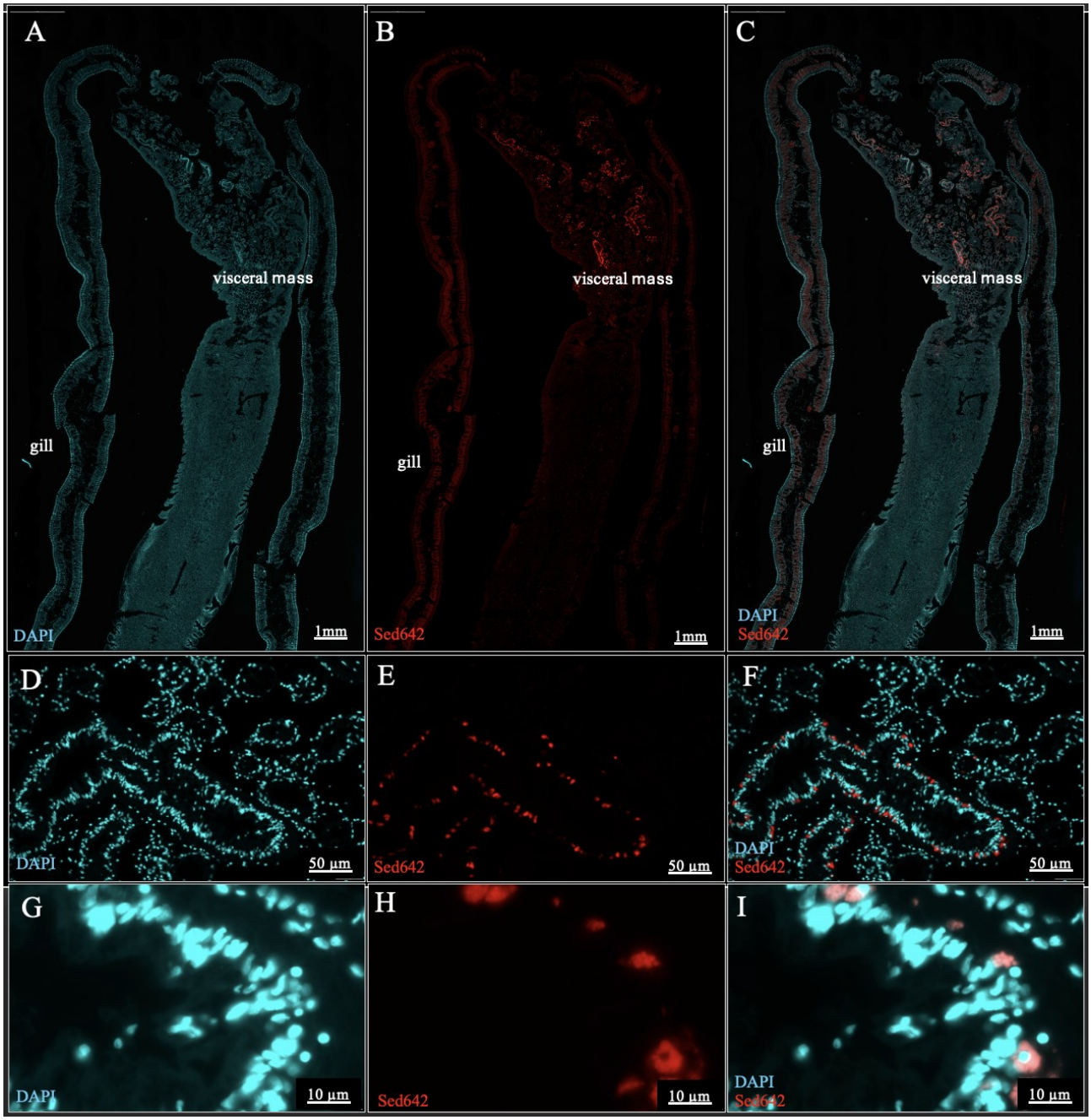

Figure 3. 3. 4. Localisation of sulphur-oxidising symbionts in *Phacoides pectinatus* detected with Sed642 probe. (A-C) Whole-body FISH image showing strong Cy3 fluorescence (red) within gill bacteriocytes, co-localised with DAPI-stained host nuclei (blue), indicating a dense intracellular symbiont population. (D-F) Magnified view of the visceral mass, where Sed642-positive bacterial cells are visible within digestive tissues, confirming symbiont presence beyond the gills. (G-I) High-magnification image of the visceral mass showing individual Sed642-positive bacterial cells within the epithelial matrix, providing clear morphological resolution of the symbiont cells.

Scale bars: A-C = 1 mm; D-F = 50 µm; G-I = 10 µm.

3. 3. 5 *Codakia orbicularis*

Hybridisation of *Codakia orbicularis* visceral mass tissue with the Sym845 probe produced distinct Cy3 fluorescence in both examined specimens (Figure 3. 3. 5A-C), (Figure 3. 3. 5D-F), indicating the presence of bacterial cells within the digestive tract region. In both individuals, the red fluorescence signal was located along the epithelial boundary of the digestive lumen and partially within luminal contents, with clear overlap between Cy3 and DAPI-stained host structures.

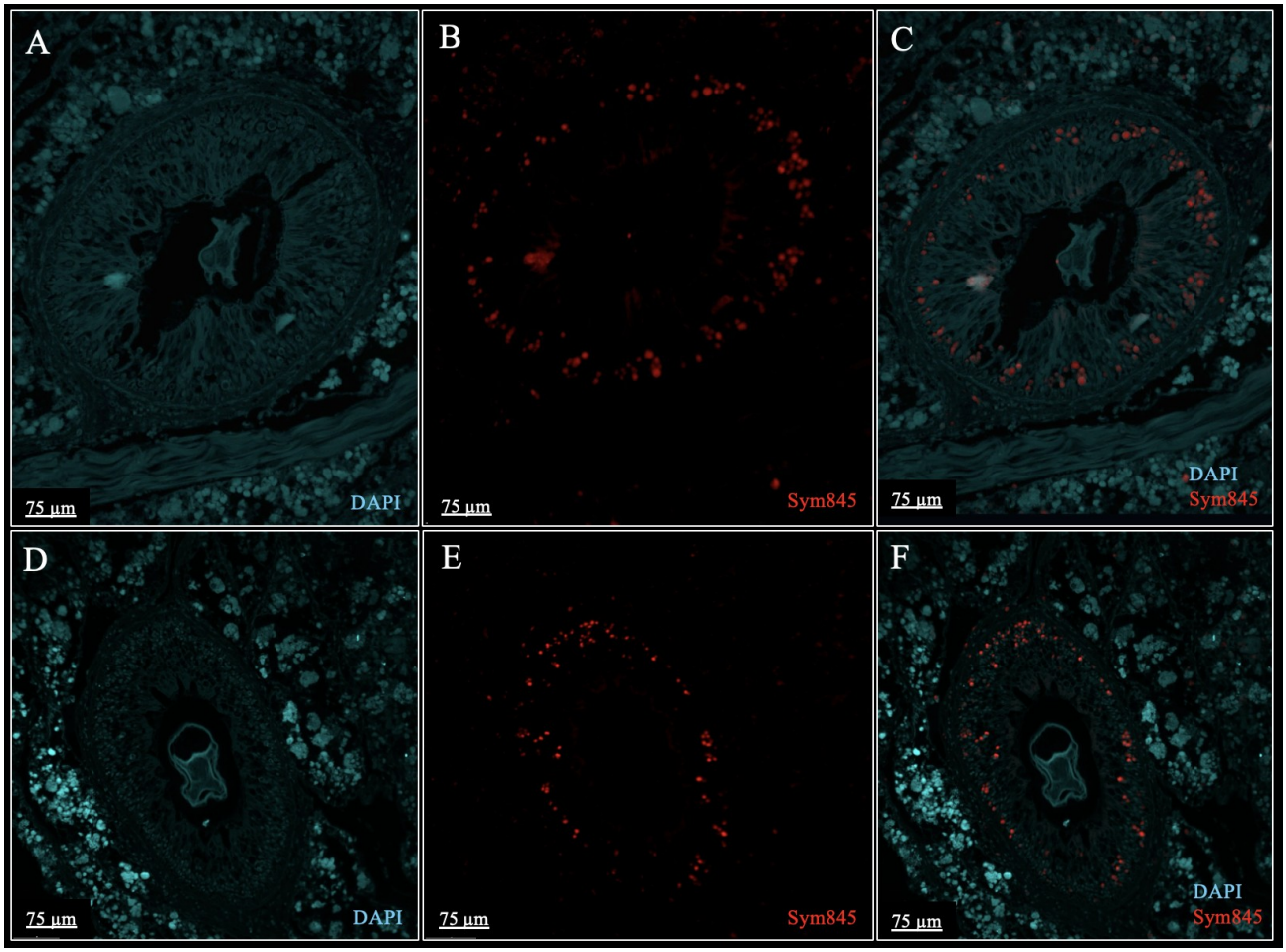

Figure 3. 3. 5. Detection of bacterial signal in visceral mass of *Codakia orbicularis*. (A-C) FISH micrograph of specimen A hybridised with the Sym845 probe (red), showing bacterial fluorescence localised along the digestive tract epithelium, with DAPI-stained host nuclei (blue) visible throughout the tissue. (D-F) An independent specimen (specimen B) displaying the same fluorescence pattern, confirming reproducibility of the visceral mass signal. Merged (DAPI + Sym845) and individual channels are shown for both specimens.

Scale bar: 75 µm.

3. 3. 6 *Solemya velum*

Hybridisation with the Svsym47 probe produced uniform, bright Cy3 fluorescence throughout the gill lamellae (Figure 3. 3. 6 A-C), reflecting the exceptionally high density of bacteriocyte-embedded, vertically transmitted symbionts in Solemyidae. The signal extended across the full lamellar width and co-localised with DAPI-stained host nuclei, indicating intracellular localisation. The usual presence of symbionts was not detected in the ovaries of *Solemaya velum* (Figure 3. 3. 6D). The foot did not display any signal of symbiont presence (Figure 3. 3. 6E).

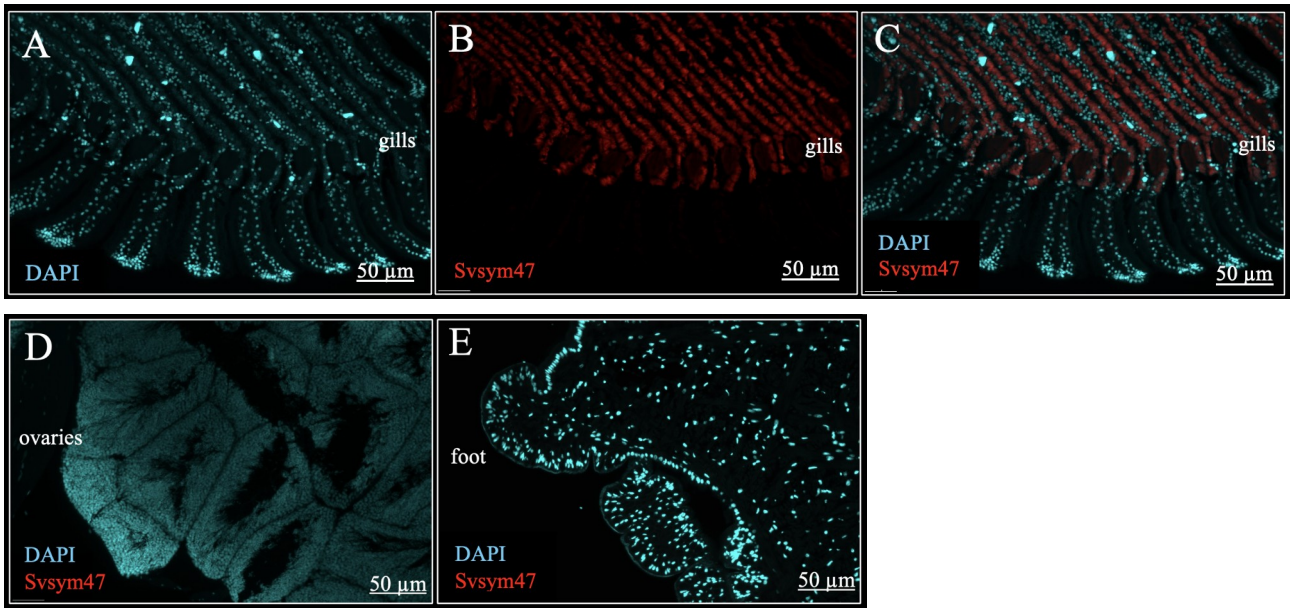

Figure 3. 3. 6. Intracellular bacterial distribution in *Solemya velum* gill tissue. (A-C) FISH micrograph of gill tissue hybridised with the Svsym47 probe (red), showing diffuse and intense fluorescence throughout the bacteriocyte layer, consistent with the exceptionally high density of intracellular symbionts characteristic of Solemyidae. DAPI (blue) labels host nuclei. (D) Ovary tissue stained with DAPI and Svsym47, showing no red fluorescence and thus no detectable Svsym47-positive bacteria. (E) Foot tissue stained with DAPI and hybridised with Svsym47, showing no red fluorescence and thus no detectable Svsym47-positive bacteria. Scale bar: 50 µm.

Discussion

4. 1 Overview

Understanding how chemosynthetic symbionts are distributed within their host tissues is fundamental to interpreting both the ecological functions and evolutionary history of chemosynthetic bivalves (Roeselers and Newton, 2012). Traditionally, lucinid symbionts have been described as strictly localised within specialised gill bacteriocytes (Frenkiel and Mouëza, 1995), while systematic studies across multiple tissues have been rare. Recent work has challenged this assumption, demonstrating that sulphur-oxidising symbionts can also occur in the digestive tract of lucinids (Alcaraz et al., 2024), suggesting that their tissue distribution may be broader than historically recognised. In this study, I tested whether this emerging model of multi-tissue colonisation applies generally across Lucinidae subfamilies by combining three complementary approaches: 16S rRNA gene sequencing, digital PCR (dPCR) targeting genes associated with sulphur oxidation, and fluorescence in situ hybridisation (FISH). These methods enabled the detection of symbiont DNA, functional sulphur oxidation marker genes, and spatial localisation within tissue, respectively. I examined four lucinid species representing different subfamilies: *Loripes orbiculatus* (Lucininae), *Loripinus fragilis* (Pegophyseminae), *Phacoides pectinatus* (Lucininae), and *Codakia orbicularis* (Codakiinae), as well as the solemyid *Solemya velum* as an evolutionary outgroup. Across lucinids, all three methods agreed on a consistent pattern: the gills contained the highest symbiont abundance, matching classical models of lucinid physiology (Fisher, 1990; Taylor & Glover, 2010). Moreover, both 16S sequencing and dPCR reproducibly detected symbiont lineages in foot, mantle, and visceral mass tissues, extending the findings of Alcaraz et al. (2024) to multiple species and subfamilies. These data show that multi-tissue symbiont presence is widespread across lucinids and is not only confined to the gills.

4. 2 Multi-tissue colonisation in Lucinidae: A conserved but variable pattern

4. 2. 1 Gill tissues as the dominant symbiont niche

Across all lucinid species studied, gills harboured the highest relative abundance of chemosynthetic symbionts, which was determined by 16S rRNA data. This is consistent with decades of histological and ultrastructural research describing dense intracellular symbiont populations within gill bacteriocytes (Distel and H. Felbeck, 1987; Taylor and Glover, 2010). FISH imaging verified this, showing strong hybridisation of lineage-specific probes (Sym845, SymAf576, Sed642) within bacteriocyte-rich lamellae. The anatomical and physiological specialisation of lucinid gills, constant water filtering, and high sulphide exposure make them optimal sites for chemosynthesis (Sogin et al., 2020; Mizutani et al., 2020). Likewise, dPCR quantifying functional sulphur-metabolism genes (*soxB, dsrC, svrhlE*) consistently showed orders of magnitude enrichment in gills relative to other tissues. This matched patterns observed in both shallow-water lucinids and deep-sea chemosynthetic bivalves (Harada et al., 2009).

4. 2. 2 Symbiont presence in non-gill tissues

Despite classical descriptions of strictly gill-limited localisation, this study consistently detected symbionts in foot, mantle, and visceral mass tissues using both 16S sequencing and dPCR. These findings are analogous to recent observations by Alcaraz et al. (2024), who documented lucinid symbionts in digestive tract tissues in *Loripes orbiculatus*. In *Loripes orbiculatus*, symbiont ASVs reached substantial proportions in foot tissues in both populations, a pattern supported by detectable but low-intensity FISH signals. *Phacoides pectinatus* exhibited a strong visceral mass signal across sequencing, dPCR, and FISH, consistent with ingestion-based acquisition pathways previously hypothesised for horizontally acquired symbionts (Roeselers and Newton, 2012). *Codakia orbicularis* showed repeated detection of symbiont ASVs in the visceral mass, which aligns with digestive tract colonisation reported in other Lucinids (Alcaraz et al., 2024). Even in species like

Loripinus fragilis, where FISH indicated strict gill localisation, low levels of symbiont DNA were still detectable in non-gill tissues via dPCR. These results, observed across three lucinid subfamilies and multiple geographic origins, strongly suggest that multi-tissue symbiont presence is biologically real rather than a sampling artefact, and may represent a widespread but previously overlooked phenomenon across Lucinidae. There are possible explanation for the outcomes. Horizontal transmission requires juveniles to acquire free-living symbionts from seawater or sediment porewater (Russell et al., 2018). Early, repeated uptake during feeding may deliver symbionts to digestive tissues, consistent with the strong visceral mass signals in *Phacoides pectinatus* and *Codakia orbicularis.* Similar initial uptake has been shown in vent tubeworms and other horizontally acquired symbioses (Ganesan et al., 2022; Bright and Bulgheresi, 2010). Several lucinid species undergo periodic symbiont loss and reacquisition, particularly following disturbances such as hypoxia or sulphide depletion (Orgeas-Gobin et al., 2025). During recolonisation, symbionts may temporarily occupy entry tissues (foot, mantle, digestive tract) before establishing in gill bacteriocytes. Lucinid visceral mass and mantle epithelium exhibit particle-capture (Duplessis et al., 2004), providing possible routes for incidental uptake of free-living symbionts. These mechanisms suggest that non-gill tissue presence is consistent with the ecology of horizontal transmission and environmental exposure.

4. 2. 3 Species-specific variation and exceptions

While multi-tissue presence was widespread, species differed from each other. *Loripes orbiculatus* showed the strongest non-gill signals. Potential explanation is its presence in shallow seagrass sediments where symbiont exposure is likely high (van der Heide et al., 2012). *Loripinus fragilis* exhibited strict gill restriction in FISH, possibly reflecting lineage-specific immune filtering or lower environmental symbiont availability (Tame, 2025). *Phacoides pectinatus* and *Codakia*

orbicularis had strong visceral mass signals, consistent with ingestion and gut-associated uptake pathways (Nguyen et al., 2013).

4. 3 Functional genes confirm the presence of true sulphur-oxidising symbionts

Digital PCR (dPCR) targeting central chemosynthetic metabolic genes, *soxB, dsrC*, and *svrhlE*, provided crucial evidence supporting that the bacteria detected in all tissues represent sulphur-oxidising symbionts. These genes are essential components of the biochemical pathways sustaining sulphur oxidising metabolism in Gammaproteobacteria (Lim et al., 2019; Venceslau et al., 2014; Stewart et al., 2011). *SoxB* encodes a periplasmic thiol dehydrogenase essential for the Sox multi enzyme complex responsible for oxidation of reduced inorganic sulphur compounds (Hensen et al., 2006). *dsrC* functions as an indispensable sulphur carrier within the reverse-dissimilatory sulphite reductase pathway, mediating electron transfer and stabilising protein-sulphur intermediates (Stockdreher et al., 2014). The RNA helicase *svrhlE*, expressed in *Solemya* symbionts, appears upregulated during active sulphur oxidation and carbon fixation, linking translational regulation with thiotrophic metabolism (Russell et al., 2018).

Because these metabolic genes are characteristic of sulphur-oxidising bacteria, their detection indicates the presence of bacteria with the genetic capacity for thiotrophic metabolism. While such genes are also widespread among free-living sulphur oxidisers in marine sediments (Friedrich et al., 2005), their consistent co-occurrence with host-specific symbiont 16S rRNA lineages, and their strong enrichment in gill tissues, supports the interpretation that the detected bacteria represent true chemosynthetic symbionts rather than incidental environmental or dietary microbes. Across lucinids, gills showed the highest functional gene copy numbers, often several orders of magnitude higher than non-gill tissues. This reflects the dense intracellular bacteriocytes described in classical ultrastructural work (Yuen et al., 2019; Frenkiel et al., 1996). However, the consistent detection of *soxB, dsrC*, and *svrhlE* in foot, mantle, and visceral mass tissues confirms that low but biologically

meaningful quantities of chemosynthetic symbionts occur outside the gills. This pattern mirrors the findings of Alcaraz et al. (2024) showing sulphur pathway genes in lucinid digestive tissues, and parallels reports of low-abundance symbionts outside primary niches in other chemosymbiotic systems (Breusing et al., 2020). Taken together, dPCR results provide crucial evidence that the symbionts detected across tissues are true sulphur-oxidisers and not incidental bacteria.

4. 4 *Solemya velum:* A contrasting pattern driven by vertical transmission

4. 4. 1 Systemic distribution of symbionts

The symbiont distribution observed in *Solemya velum* differs from the patterns found in lucinids, reflecting its contrasting symbiont transmission strategy. While lucinids rely exclusively on horizontal acquisition from the environment (Gros et al., 2012), Solemyidae transmit their symbionts vertically via the egg cytoplasm (Russell et al., 2018). Vertical transmission results in early-life systemic symbiont presence, with symbionts permeating tissues before becoming concentrated within gill bacteriocytes (Bright and Bulgheresi, 2010; Russell et al., 2018). This developmental pattern was strongly reflected in the present results. FISH imaging showed dense and diffuse symbiont signal throughout the entire gill bacteriocyte zone, consistent with the high intracellular symbiont loads characteristic of *Solemaya velum* (Russell et al., 2018). dPCR further revealed high *svrhlE* copy numbers across tissues. In contrast to previous studies that have documented symbiont presence in the ovaries of *Solemaya velum* (Russell et al., 2018), the current dataset did not detect symbiont-specific signals in ovarian tissue using FISH. Instead, only background bacterial DNA was observed, and no hybridisation with symbiont-targeted probes occurred. Several explanations are possible: (i) low symbiont abundance in the sampled reproductive stage, (ii) degradation of ovarian tissue prior to fixation, or (iii) natural variability in reproductive cycling (Russell et al., 2018). Regardless of cause, the absence of ovarian detection in

this study should not be interpreted as contradictory to the established vertical transmission model, but rather as a reminder that symbiont abundance in reproductive tissues may fluctuate.

4. 4. 2 Implications for the evolution of symbiont localisation

The comparison between horizontally acquired lucinid symbioses and vertically transmitted solemyid symbioses provides insights into how transmission strategy shapes anatomical localisation. Horizontally transmitted systems tend to favour compartmentalisation into specialised tissues, likely as a mechanism to regulate symbiont entry, manage immune interactions, and optimise metabolic exchange (Bright & Bulgheresi, 2010; Chomicki et al., 2020). In contrast, vertically transmitted systems inherently begin with broader anatomical distribution, often retaining the capacity for early systemic colonisation well into adult life stages (Tanger et al., 2024). Thus, the combination of concentrated gill signal and ovarian symbiont presence in *Solemaya velum* reflects the deep evolutionary divergence between these lineages (Russell et al., 2018). The lucinid pattern of multi-tissue but low-density symbiont presence may represent transient uptake or recolonisation pathways.

4. 5 Integrative interpretation of FISH, 16S, and dPCR across tissues

4. 5. 1 Strong convergence across sequencing-based methods

A major finding of this study is the strong agreement between *16S rRNA* gene sequencing and dPCR quantification across nearly all species and tissues. Both methods consistently detected sulphur-oxidising symbiont lineages in gills and at lower abundance in non-gill tissues, reflecting the power of DNA-based methods to detect rare symbionts that may be physiologically or anatomically sparse (Hugerth & Andersson, 2017; Lee et al., 2022). The co-occurrence of high 16S ASV abundance and elevated *soxB/dsrC/svrhlE* gene copies in gills confirms that these tissues harbour the major metabolically active symbiont population. The agreement between sequencing and dPCR in foot and visceral mass tissues, especially in *Loripes orbiculatus* and *Phacoides*

pectinatus, strongly supports the fact of multi-tissue colonisation beyond gills. These patterns indicate that both methods reliably detect symbiont DNA within and outside the primary symbiotic organ.

4. 5. 2 FISH as the most restrictive detection method

In contrast to the broad detection achieved through sequencing and dPCR, FISH hybridisation identified symbionts primarily in gill tissues, with medium-intensity detection outside the gills. This discrepancy highlights FISH as the most restrictive and least sensitive of the three methods. FISH requires high rRNA content and sufficient cell density to generate a visible signal (Hoshino et al., 2008). Low-abundance symbionts, especially those transiently present or metabolically inactive, would fall below this threshold (Wendeberg, 2010). Probe penetration also varies dramatically between tissues (Pernthaler and Amann, 2004). Tissue autofluorescence is another confounding factor, especially in digestive organs, where natural pigments can obscure weak signals (Ainsworth et al., 2008). Thus, the absence of FISH signals in non-gill tissues should be interpreted conservatively and does not contradict the molecular evidence. Instead, the mismatch reflects the lower sensitivity of FISH relative to sequencing and dPCR.

4. 5. 3 Strength of multi-method approach

By integrating three complementary methods, this study provides a robust multidimensional picture of symbiont distribution. The consistent agreement between sequencing and dPCR gives strong confidence that the observed non-gill symbiont signals are biologically meaningful. Meanwhile, the FISH data reliably confirm the anatomical localisation of dense symbiont populations in gills while highlighting the limited detectability of sparse cells in other tissues. Here, the agreement of two independent molecular detection approaches together with microscopic evidence strongly supports the interpretation that low-level symbiont presence outside gills is a real and widespread feature of lucinid biology. These findings also contribute to broader theoretical models of chemosynthetic

mutualism. Traditionally, chemosymbioses have been framed as highly compartmentalised and anatomically constrained systems, particularly in horizontally transmitted bivalves (Petersen and Yuen, 2021). The consistent multi-tissue presence documented here challenges this view and suggests that chemosynthetic partnerships may be more spatially dynamic than previously recognised. This dispersed colonisation may facilitate resilience during environmental fluctuations and permit recolonisation following symbiont loss, thereby functioning as an adaptive cushion in variable sedimentary environments.

4. 6 Limitations of the present study

Despite the robustness of the multi-method approach, several biological and methodological limitations must be acknowledged to appropriately contextualise the findings. A significant limitation is the relatively small number of individuals analysed per species. Symbiont density varies with environmental conditions. Sulphide availability, seagrass oxygenation, temperature, and host nutritional state contribute to variable symbiont density (Orgeas-Gobin et al., 2025; Conte et al., 2021). Without broader sampling across seasons, it remains unclear whether the patterns reported here represent stable species-level features or season-dependent dynamics. For instance, lucinids clams undergoes marked seasonal changes in symbiont load (Orgeas-Gobin et al., 2025), meaning that sampling at a single time point may capture only one phase of an annual cycle. Additionally, the study did not include larval or early juvenile stages. These are critical for understanding initial symbiont acquisition and could clarify whether non-gill tissues function as primary colonisation sites during early development (Suzuki et al., 2013). Each methodological approach also imply specific constraints. 16S rRNA amplicon sequencing, while sensitive, is prone to primer bias, limited taxonomic resolution, and underrepresentation of low-abundance taxa (Srinivas et al., 2025). It cannot distinguish between intracellular and extracellular bacteria nor between viable and non-viable cells (Yap et al., 2022). FISH demonstrated the greatest limitations

in this study. It requires high rRNA content for detection (Hoshino et al., 2008) and thus biased detection of metabolically inactive or low-density symbionts. dPCR quantifies gene copies but cannot differentiate living from dead bacteria or free DNA from intracellular cells (Soejima et al., 2008). Finally, cross-contamination during dissection is a potential concern, especially when working with very small tissues (Asor et al., 2017). Nevertheless, the strong concordance between 16S and dPCR data, combined with the clear gill-specific patterning revealed by FISH, suggests that the observed multi-tissue signals are unlikely to be solely artefactual, despite the acknowledged limitations. The methodologies employed detect DNA or rRNA, which do not unequivocally demonstrate metabolic activity. Without transcriptomics or metabolomics, it remains unresolved whether symbionts detected in non-gill tissues are active, dormant, or recently ingested. Thus, while the evidence strongly supports multi-tissue symbiont presence, the functional relevance of this presence remains to be experimentally determined.

4. 7 Future work

To build on the findings of this thesis, several methodological and analytical improvements are necessary to improve our understanding of tissue-level symbiont distribution in chemosynthetic bivalves. First, optimisation of FISH probe specificity and hybridisation conditions should be prioritised. This is particularly relevant for *Codakia orbicularis* and *Loripinus fragilis*, where probe performance was weaker or produced ambiguous signals. Enhanced probe design or multiplexed hybridisation strategies may substantially improve detection sensitivity. Second, more comprehensive imaging of *Codakia orbicularis* tissues, especially the gill and foot, will be essential for confirming localisation patterns beyond the visceral mass. Third, expanding biological replication to approximately ten individuals per species would allow statistically robust comparisons across tissues and lineages. This could minimise the influence of individual-level variability. Finally, now that symbiont presence in non-gill tissues has been consistently

documented using molecular methods, future research should directly assess whether these populations are metabolically active or merely transient. Approaches such as spatial transcriptomics, stable isotope probing, or nanoscale secondary ion mass spectrometry (NanoSIMS) will be critical for evaluating the functional significance of non-gill symbionts. Combination of these techniques could determine whether they participate in the host's chemosynthetic metabolism.

4. 8 Conclusion

This study provides a comprehensive multi-tissue characterisation of chemosynthetic symbiont distribution in lucinid bivalves to date. It also integrates 16S rRNA gene profiling, digital PCR of sulphur-metabolism genes, and high-resolution FISH microscopy. Across all lucinid species, gills consistently housed dense populations of sulphur-oxidising symbionts. This outcome reaffirms their role as the primary site of chemosynthetic activity. Nevertheless, the recurrent detection of symbiont DNA and/or rRNA in foot, mantle, and visceral mass tissues shows that lucinid symbiont presence is broader and more dynamic than previously thought. These findings demonstrate that low-level, multi-tissue colonisation is conserved, but species-specific. Moreover, it is a feature of horizontally transmitted symbioses, likely reflecting environmental acquisition processes, epithelial uptake, or transient recolonisation pathways. In contrast, *Solemya velum* displayed a different pattern, with systemic symbiont presence linked to vertical transmission. The difference between the evolutionary groups highlights deep evolutionary divergence in host-microbe interactions between Lucinidae and Solemyidae. These results expand the classical view of bivalve chemosymbiosis from a strictly gill-centred dogma to a more flexible, host-wide interaction. The work not only provides updated information for understanding symbiont localisation but also highlights the need for future research integrating developmental, ultrastructural, and functional genomic approaches. These approaches could aim to determine whether non-gill symbionts represent transient environmental stages, early colonisation intermediates, or previously overlooked

components of chemosynthetic mutualism. Altogether, these findings directly address the central aim of this thesis: to determine whether multi-tissue symbiont presence is a generalised or lineage-specific feature of lucinid bivalves.

References

1. Ainsworth, T.D., Hoegh-Guldberg, O. and Leggat, W. (2008). Imaging the fluorescence of marine invertebrates and their associated flora. Journal of Microscopy, 232(2), pp.197-199. doi:https://doi.org/10.1111/j.1365-2818.2008.02089.x.
2. Alcaraz, C.M., Séneca, J., Kunert, M., Pree, C., Sudo, M. and Petersen, J.M. (2024). Sulfur-oxidizing symbionts colonize the digestive tract of their Lucinid hosts. The ISME Journal, 18(1). doi:https://doi.org/10.1093/ismejo/wrae200.
3. Asor, E., Stav, M.Y., Simon, E., Fahoum, I., Sabo, E., Ben-Izhak, O. and Hershkovitz, D. (2017). Risk for molecular contamination of tissue samples evaluated for targeted anti-cancer therapy. PLOS ONE, 12(3), p.e0173760. doi:https://doi.org/10.1371/journal.pone.0173760.
4. Barnett, D., Arts, I. and Penders, J. (2021). microViz: an R package for microbiome data visualization and statistics. Journal of Open Source Software, 6(63), p.3201. doi:https://doi.org/10.21105/joss.03201.
5. Béziat, N.S., Duperron, S. and Gros, O. (2024). Environmental Transmission of Symbionts in the Mangrove Crabs *Aratus pisonii* and *Minuca rapax*: Acquisition of the Bacterial Community through Larval Development to Juvenile Stage. Microorganisms, [online] 12(4), pp.652-652. doi:https://doi.org/10.3390/microorganisms12040652.
6. Breusing, C., Mitchell, J., Delaney, J., Sylva, S.P., Seewald, J.S., Girguis, P.R. and Beinart, R.A. (2020). Physiological dynamics of chemosynthetic symbionts in hydrothermal vent snails. The ISME Journal, 14(10), pp.2568-2579. doi:https://doi.org/10.1038/s41396-020-0707-2.
7. Bright, M. and Bulgheresi, S. (2010). A complex journey: transmission of microbial symbionts. Nature Reviews Microbiology, 8(3), pp.218-230. doi:https://doi.org/10.1038/nrmicro2262.
8. Brissac, T., Higuet, D., Gros, O. and Merçot, H. (2016). Unexpected structured intraspecific diversity of thioautotrophic bacterial gill endosymbionts within the Lucinidae (Mollusca: Bivalvia). Marine Biology, 163(8). doi:https://doi.org/10.1007/s00227-016-2949-0.

9. Callahan, B.J., McMurdie, P.J., Rosen, M.J., Han, A.W., Johnson, A.J.A. and Holmes, S.P. (2016a). DADA2: High-resolution sample inference from Illumina amplicon data. Nature Methods, 13(7), pp.581-583. doi:https://doi.org/10.1038/nmeth.3869.
10. Callahan, B.J., Sankaran, K., Fukuyama, J.A., McMurdie, P.J. and Holmes, S.P. (2016b). Bioconductor Workflow for Microbiome Data Analysis: from raw reads to community analyses. F1000Research, 5, p.1492. doi:https://doi.org/10.12688/f1000research.8986.2.
11. Chin, D.W., Fouw, J., Heide, T., Cahill, B.V., Katcher, K., Paul, V.J., Campbell, J.E. and Peterson, B.J. (2020). Facilitation of a tropical seagrass by a chemosymbiotic bivalve increases with environmental stress. Journal of Ecology, 109(1), pp.204-217. doi:https://doi.org/10.1111/1365-2745.13462.
12. Chomicki, G., Werner, G.D.A., West, S.A. and Kiers, E.T. (2020). Compartmentalization drives the evolution of symbiotic cooperation. Philosophical Transactions of the Royal Society B: Biological Sciences, 375(1808), p.20190602. doi:https://doi.org/10.1098/rstb.2019.0602.
13. Conte, C., Rotini, A., Manfra, L., D'Andrea, M.M., Winters, G. and Migliore, L. (2021). The Seagrass Holobiont: What We Know and What We Still Need to Disclose for Its Possible Use as an Ecological Indicator. Water, 13(4), p.406. doi:https://doi.org/10.3390/w13040406.
14. Davis, N.M., Proctor, D.M., Holmes, S.P., Relman, D.A. and Callahan, B.J. (2018). Simple statistical identification and removal of contaminant sequences in marker-gene and metagenomics data. Microbiome, 6(1). doi:https://doi.org/10.1186/s40168-018-0605-2.
15. de Fouw, J., Govers, Laura L., van de Koppel, J., van Belzen, J., Dorigo, W., Sidi Cheikh, Mohammed A., Christianen, Marjolijn J.A., van der Reijden, Karin J., van der Geest, M., Piersma, T., Smolders, Alfons J.P., Olff, H., Lamers, Leon P.M., van Gils, Jan A. and van der Heide, T. (2016). Drought, Mutualism Breakdown, and Landscape-Scale Degradation of Seagrass Beds. Current Biology, 26(8), pp.1051-1056. doi:https://doi.org/10.1016/j.cub.2016.02.023.

16. Distel, D.L. and H. Felbeck (1987). Endosymbiosis in the lucinid clams *Lucinoma aequizonata*, *Lucinoma annulata* and *Lucina floridana*: a reexamination of the functional morphology of the gills as bacteria-bearing organs. Marine Biology, 96(1), pp.79-86. doi:https://doi.org/10.1007/bf00394840.

17. Dubilier, N., Bergin, C. and Lott, C. (2008). Symbiotic diversity in marine animals: the art of harnessing chemosynthesis. Nature Reviews Microbiology, 6(10), pp.725-740. doi:https://doi.org/10.1038/nrmicro1992.

18. Duperron, S., Gaudron, S.M., Rodrigues, C.F., Cunha, M.R., Decker, C. and Olu, K. (2013). An overview of chemosynthetic symbioses in bivalves from the North Atlantic and Mediterranean Sea. Biogeosciences, 10(5), pp.3241-3267. doi:https://doi.org/10.5194/bg-10-3241-2013.

19. Duplessis, M.R., Dufour, S.C., Blankenship, L.E., H. Felbeck and Yayanos, A.A. (2004). Anatomical and experimental evidence for particulate feeding in *Lucinoma aequizonata* and *Parvilucina tenuisculpta* (Bivalvia: Lucinidae) from the Santa Barbara Basin. Marine Biology, 145(3). doi:https://doi.org/10.1007/s00227-004-1350-6.

20. Friedrich, C.G., Bardischewsky, F., Rother, D., Quentmeier, A. and Fischer, J. (2005). Prokaryotic sulfur oxidation. Current Opinion in Microbiology, 8(3), pp.253-259. doi:https://doi.org/10.1016/j.mib.2005.04.005.

21. Ganesan, R., Wierz, J.C., Kaltenpoth, M. and Flórez, L.V. (2022). How It All Begins: Bacterial Factors Mediating the Colonization of Invertebrate Hosts by Beneficial Symbionts. Microbiology and molecular biology reviews, 86(4). doi:https://doi.org/10.1128/mmbr.00126-21.

22. Github.io. (2025). Home - miaverse. [online] Available at: https://microbiome.github.io [Accessed 9 Dec. 2025].

23. Gros, O., Elisabeth, N.H., Gustave, S.D.D., Caro, A. and Dubilier, N. (2012). Plasticity of symbiont acquisition throughout the life cycle of the shallow-water tropical lucinid *Codakia*

orbiculata (Mollusca: Bivalvia). Environmental Microbiology, 14(6), pp.1584-1595. doi:https://doi.org/10.1111/j.1462-2920.2012.02748.x.

24. Harada, M., Yoshida, T., Kuwahara, H., Shimamura, S., Takaki, Y., Kato, C., Miwa, T., Miyake, H. and Maruyama, T. (2009). Expression of genes for sulfur oxidation in the intracellular chemoautotrophic symbiont of the deep-sea bivalve *Calyptogena okutanii*. Extremophiles, 13(6), pp.895-903. doi:https://doi.org/10.1007/s00792-009-0277-8.
25. Hensen, D., Sperling, D., Trüper, H.G., Brune, D.C. and Dahl, C. (2006). Thiosulphate oxidation in the phototrophic sulphur bacterium *Allochromatium vinosum*. Molecular Microbiology, 62(3), pp.794-810. doi:https://doi.org/10.1111/j.1365-2958.2006.05408.x.
26. Hoshino, T., Yilmaz, L.S., Noguera, D.R., Daims, H. and Wagner, M. (2008). Quantification of Target Molecules Needed To Detect Microorganisms by Fluorescence In Situ Hybridization (FISH) and Catalyzed Reporter Deposition-FISH. Applied and Environmental Microbiology, 74(16), pp.5068-5077. doi:https://doi.org/10.1128/aem.00208-08.
27. Huang, R., Soneson, C., Ernst, F.G.M., Rue-Albrecht, K.C., Yu, G., Hicks, S.C. and Robinson, M.D. (2020). TreeSummarizedExperiment: a S4 class for data with hierarchical structure. F1000Research, 9, p.1246. doi:https://doi.org/10.12688/f1000research.26669.1.
28. Chi-Ho Ip, J., Xu, T., Sun, J., Li, R., Chen, C., Lan, Y., Han, Z., Zhang, H., Wei, J., Wang, H., Tao, J., Cai, Z., Qian, P.-Y. and Qiu, J.-W. (2020). Host-Endosymbiont Genome Integration in a Deep-Sea Chemosymbiotic Clam. Molecular Biology and Evolution, 38(2), pp.502-518. doi:https://doi.org/10.1093/molbev/msaa241.
29. Järnegren, J. and Altin, D. (2006). Filtration and respiration of the deep living bivalve *Acesta excavata* (J.C. Fabricius, 1779) (Bivalvia; Limidae). Journal of Experimental Marine Biology and Ecology, [online] 334(1), pp.122-129. doi:https://doi.org/10.1016/j.jembe.2006.01.014.
30. Klindworth, A., Pruesse, E., Schweer, T., Peplies, J., Quast, C., Horn, M. and Glöckner, F.O. (2012). Evaluation of general 16S ribosomal RNA gene PCR primers for classical and next-

generation sequencing-based diversity studies. Nucleic Acids Research, [online] 41(1), pp.e1-e1. doi:https://doi.org/10.1093/nar/gks808.

31. Krueger, D.M., Gustafson, R.G. and Cavanaugh, C.M. (1996). Vertical Transmission of Chemoautotrophic Symbionts in the Bivalve *Solemya velum* (Bivalvia: Protobranchia). The Biological Bulletin, 190(2), pp.195-202. doi:https://doi.org/10.2307/1542539.
32. Frenkiel, L., Gros, O. and Mouëza, M. (1996). Gill structure in *Lucina pectinata* (Bivalvia: Lucinidae) with reference to hemoglobin in bivalves with symbiotic sulphur-oxidizing bacteria. Marine Biology, 125(3), pp.511-524. doi:https://doi.org/10.1007/bf00353264.
33. Frenkiel, M. and Mouëza M. (1995). Gill ultrastructure and symbiotic bacteria in *Codakia orbicularis* (Bivalvia, Lucinidae). Zoomorphology, 115(1), pp.51–61. doi:https://doi.org/10.1007/bf00397934.
34. Lim, S.J., Davis, B.G., Gill, D.E., Walton, J., Nachman, E., Engel, A.S., Anderson, L.C. and Campbell, B.J. (2019). Taxonomic and functional heterogeneity of the gill microbiome in a symbiotic coastal mangrove lucinid species. The ISME Journal, [online] 13(4), pp.902–920. doi:https://doi.org/10.1038/s41396-018-0318-3.
35. Martin, B.C., Middleton, J.A., Fraser, M.W., Marshall, I.P.G., Scholz, V.V., Hausl, B. and Schmidt, H. (2020). Cutting out the middle clam: lucinid endosymbiotic bacteria are also associated with seagrass roots worldwide. The ISME Journal, [online] 14(11), pp.2901-2905. doi:https://doi.org/10.1038/s41396-020-00771-3.
36. McLaren, M.R. and Callahan, B.J. (2021). Silva 138.1 prokaryotic SSU taxonomic training data formatted for DADA2. [online] Zenodo. doi:https://doi.org/10.5281/zenodo.4587955.
37. McMurdie, P.J. and Holmes, S. (2013). phyloseq: An R Package for Reproducible Interactive Analysis and Graphics of Microbiome Census Data. PLoS ONE, 8(4), p.e61217. doi:https://doi.org/10.1371/journal.pone.0061217.

38. Mizutani, Y., Mori, T., Miyazaki, T., Fukuzaki, S. and Tanaka, R. (2020). Microbial community analysis in the gills of abalones suggested possible dominance of epsilonproteobacterium in *Haliotis gigantea*. PeerJ, 8, p.e9326. doi:https://doi.org/10.7717/peerj.9326.

39. Moran, N.A. (2007). Symbiosis as an Adaptive Process and Source of Phenotypic Complexity. [online] www.ncbi.nlm.nih.gov. National Academies Press (US). Available at: https://www.ncbi.nlm.nih.gov/books/NBK254296/ [Accessed 20 Nov. 2022].

40. Morton, B. (2024). Bivalve | class of mollusks. [online] Encyclopedia Britannica. Available at: https://www.britannica.com/animal/bivalve.

41. Nguyen, M.T.H.D., Liu, M. and Thomas, T. (2013). Ankyrin-repeat proteins from sponge symbionts modulate amoebal phagocytosis. Molecular Ecology, 23(6), pp.1635-1645. doi:https://doi.org/10.1111/mec.12384.

42. Orgeas-Gobin, S., Piquet, B., Marie, B., Andersen, A., Tanguy, A. and Duperron, S. (2025). Symbiont retention and holobiont response under simulated sulfide deprivation in Lucinid clams from seagrass beds. Frontiers in Microbiology, 16. doi:https://doi.org/doi.org/10.3389/fmicb.2025.1637201.

43. Osvatic, J.T., Yuen, B., Kunert, M., Wilkins, E., Hausmann, B., Girguis, P.R., Lundin, K., Taylor, J.D., Guillaume Jospin and Petersen, J.M. (2023). Gene loss and symbiont switching during adaptation to the deep sea in a globally distributed symbiosis. The ISME Journal, 17(3), pp.453-466. doi:https://doi.org/10.1038/s41396-022-01355-z.

44. Pawlowska, T.E. (2024). Symbioses between fungi and bacteria: from mechanisms to impacts on biodiversity. Current Opinion in Microbiology, [online] 80, p.102496. doi:https://doi.org/10.1016/j.mib.2024.102496.

45. Pernthaler, A. and Amann, R. (2004). Simultaneous Fluorescence In Situ Hybridization of mRNA and rRNA in Environmental Bacteria. Applied and Environmental Microbiology, 70(9), pp.5426-5433. doi:https://doi.org/10.1128/aem.70.9.5426-5433.2004.

46. Petersen, J.M., Kemper, A., Gruber-Vodicka, H., Cardini, U., van der Geest, M., Kleiner, M., Bulgheresi, S., Mußmann, M., Herbold, C., Seah, B.K.B., Antony, C.P., Liu, D., Belitz, A. and Weber, M. (2016). Chemosynthetic symbionts of marine invertebrate animals are capable of nitrogen fixation. Nature Microbiology, [online] 2(1), pp.1-11. doi:https://doi.org/10.1038/nmicrobiol.2016.195.

47. Petersen, J.M. and Yuen, B. (2021). The Symbiotic 'All-Rounders': Partnerships between Marine Animals and Chemosynthetic Nitrogen-Fixing Bacteria. Applied and Environmental Microbiology, 87(5). doi:https://doi.org/10.1128/aem.02129-20.

48. Pjevac, P., Hausmann, B., Schwarz, J., Kohl, G., Herbold, C.W., Loy, A. and Berry, D. (2021). An Economical and Flexible Dual Barcoding, Two-Step PCR Approach for Highly Multiplexed Amplicon Sequencing. Frontiers in Microbiology, [online] 12, p.669776. doi:https://doi.org/10.3389/fmicb.2021.669776.

49. Quast, C., Pruesse, E., Yilmaz, P., Gerken, J., Schweer, T., Yarza, P., Peplies, J. and Glöckner, F.O. (2012). The SILVA Ribosomal RNA Gene Database project: Improved Data Processing and web-based Tools. Nucleic Acids Research, 41(D1), pp.D590-D596. doi:https://doi.org/10.1093/nar/gks1219.

50. Reynolds, L.K., Berg, P. and Zieman, J.C. (2007). Lucinid clam influence on the biogeochemistry of the seagrass *Thalassia testudinum* sediments. Estuaries and Coasts, 30(3), pp.482-490. doi:https://doi.org/10.1007/bf02819394.

51. Roeselers, G. and Newton, I.L.G. (2012). On the evolutionary ecology of symbioses between chemosynthetic bacteria and bivalves. Applied Microbiology and Biotechnology, 94(1), pp.1-10. doi:https://doi.org/10.1007/s00253-011-3819-9.

52. Rueda, J.L. and Salas, C. (2008). Molluscs associated with a subtidal *Zostera marina L.* bed in southern Spain: Linking seasonal changes of fauna and environmental variables. Estuarine Coastal and Shelf Science, 79(1), pp.157-167. doi:https://doi.org/10.1016/j.ecss.2008.03.018.

53. Russell, S.L., McCartney, E. and Cavanaugh, C.M. (2018). Transmission strategies in a chemosynthetic symbiosis: detection and quantification of symbionts in host tissues and their environment. Proceedings - Royal Society. Biological sciences/Proceedings - Royal Society. Biological Sciences, 285(1890), pp.20182157-20182157. doi:https://doi.org/10.1098/rspb.2018.2157.

54. Soejima, T., Iida, K., Qin, T., Taniai, H., Seki, M. and Yoshida, S. (2008). Method To Detect Only Live Bacteria during PCR Amplification. Journal of Clinical Microbiology, [online] 46(7), pp.2305-2313. doi:https://doi.org/10.1128/JCM.02171-07.

55. Sogin, E.M., Leisch, N. and Dubilier, N. (2020). Chemosynthetic symbioses. Current Biology, 30(19), pp.R1137-R1142. doi:https://doi.org/10.1016/j.cub.2020.07.050.

56. Srinivas, M., Walsh, C.J., Crispie, F., Orla O'Sullivan, Cotter, P.D., Douwe van Sinderen and Kenny, J.G. (2025). Evaluating the efficiency of 16S-ITS-23S operon sequencing for species level resolution in microbial communities. Scientific Reports, 15(1). doi:https://doi.org/10.1038/s41598-024-83410-7.

57. Stanley, S.M. (2014). Evolutionary radiation of shallow-water Lucinidae (Bivalvia with endosymbionts) as a result of the rise of seagrasses and mangroves. Geology, 42(9), pp.803-806. doi:https://doi.org/10.1130/g35942.1.

58. Stewart, F.J., Dmytrenko, O., DeLong, E.F. and Cavanaugh, C.M. (2011). Metatranscriptomic Analysis of Sulfur Oxidation Genes in the Endosymbiont of *Solemya Velum*. Frontiers in Microbiology, 2. doi:https://doi.org/10.3389/fmicb.2011.00134.

59. Stewart, F.J., Newton, I.L.G. and Cavanaugh, C.M. (2005). Chemosynthetic endosymbioses: adaptations to oxic-anoxic interfaces. Trends in Microbiology, 13(9), pp.439-448. doi:https://doi.org/10.1016/j.tim.2005.07.007.

60. Stockdreher, Y., Sturm, M., Josten, M., Sahl, H.-G., Dobler, N., Zigann, R. and Dahl, C. (2014). New Proteins Involved in Sulfur Trafficking in the Cytoplasm of *Allochromatium vinosum*. 289(18), pp.12390-12403. doi:https://doi.org/10.1074/jbc.m113.536425.

61. Sudo, M., Osvatic, J., Taylor, J.D., Dufour, S.C., Anchana Prathep, Wilkins, E., Rattei, T., Yuen, B. and Petersen, J.M. (2024). *SoxY* gene family expansion underpins adaptation to diverse hosts and environments in symbiotic sulfide oxidizers. mSystems, 9(6), pp.e0113523-e0113523. doi:https://doi.org/10.1128/msystems.01135-23.

62. Suzuki, G., Yamashita, H., Kai, S., Hayashibara, T., Suzuki, K., Iehisa, Y., Okada, W., Ando, W. and Komori, T. (2013). Early uptake of specific symbionts enhances the post-settlement survival of Acropora corals. Marine Ecology Progress Series, 494, pp.149-158. doi:https:// doi.org/10.3354/meps10548.

63. Tame, A. (2025). Integrated Regulation of Immunity and Nutritional Symbiosis in Deep-Sea Mussels. Marine Drugs, 23(11), pp.425-425. doi:https://doi.org/10.3390/md23110425.

64. Tanger, I.S., Stefanschitz, J., Schwert, Y. and Roth, O. (2024). The source of microbial transmission influences niche colonization and microbiome development. Proceedings of the Royal Society B Biological Sciences, 291(2016). doi:https://doi.org/10.1098/rspb.2023.2036.

65. Taylor, J.D., and Glover, E.A. (2021). Biology, evolution and generic review of the chemosymbiotic bivalve family Lucinidae. London: Ray Society.

66. Taylor, J.D. and Glover, E.A. (2010). Chemosymbiotic Bivalves. Topics in geobiology, pp.107-135. doi:https://doi.org/10.1007/978-90-481-9572-5_5.

67. Taylor, J.D. and Glover, E.A. (2005). Cryptic diversity of chemosymbiotic bivalves: A systematic revision of worldwide Anodontia (Mollusca: Bivalvia: Lucinidae). Systematics and Biodiversity, 3(3), pp.281-338. doi:https://doi.org/10.1017/s1477200005001672.

68. Taylor, J.D., Glover, E.A., Smith, L., Dyal, P. and Williams, S.T. (2011). Molecular phylogeny and classification of the chemosymbiotic bivalve family Lucinidae (Mollusca: Bivalvia).

Zoological Journal of the Linnean Society, 163(1), pp.15–49. doi:https://doi.org/10.1111/j.1096-3642.2011.00700.x.

69. Tucker Abbott, R. (2001). A Field Guide to Shells : Atlantic and Gulf Coasts and the West Indies. Houghton Mifflin (P.
70. van der Heide, T., Govers, L.L., de Fouw, J., Olff, H., van der Geest, M., van Katwijk, M.M., Piersma, T., van de Koppel, J., Silliman, B.R., Smolders, A.J.P. and van Gils, J.A. (2012). A Three-Stage Symbiosis Forms the Foundation of Seagrass Ecosystems. Science, 336(6087), pp.1432-1434. doi:https://doi.org/10.1126/science.1219973.
71. Venceslau, S.S., Stockdreher, Y., Dahl, C. and Pereira, I.A.C. (2014). The 'bacterial heterodisulfide' *DsrC* is a key protein in dissimilatory sulfur metabolism. Biochimica et Biophysica Acta (BBA) - Bioenergetics, 1837(7), pp.1148-1164. doi:https://doi.org/10.1016/j.bbabio.2014.03.007.
72. Walker, W.F. and Barnes, R.D. (1991). Zoology. Phihladelphia: Saunders College Publishing.
73. Wendeberg, A. (2010). Fluorescence In Situ Hybridization for the Identification of Environmental Microbes. Cold Spring Harbor Protocols, 2010(1), pp.pdb.prot5366-pdb.prot5366. doi:https://doi.org/10.1101/pdb.prot5366.
74. Xu, L.L., Chen, H., Zhang, M., Zhu, W., Chang, Q., Lu, G., Chen, Y., Jiang, J. and Zhu, L. (2020). Changes in the community structure of the symbiotic microbes of wild amphibians from the eastern edge of the Tibetan Plateau. MicrobiologyOpen, 9(4). doi:https://doi.org/10.1002/mbo3.1004.
75. Yap, M., Órla O'Sullivan, O'Toole, P.W. and Cotter, P.D. (2022). Development of sequencing-based methodologies to distinguish viable from non-viable cells in a bovine milk matrix: A pilot study. Frontiers in Microbiology, 13. doi:https://doi.org/10.3389/fmicb.2022.1036643.
76. Yuen, B., Polzin, J. and Petersen, J.M. (2019). Organ transcriptomes of the lucinid clam *Loripes orbiculatus* (Poli, 1791) provide insights into their specialised roles in the biology of a

chemosymbiotic bivalve. BMC Genomics, 20(1). doi:https://doi.org/10.1186/s12864-019-6177-0.

Supplementary information

Supplementary figures

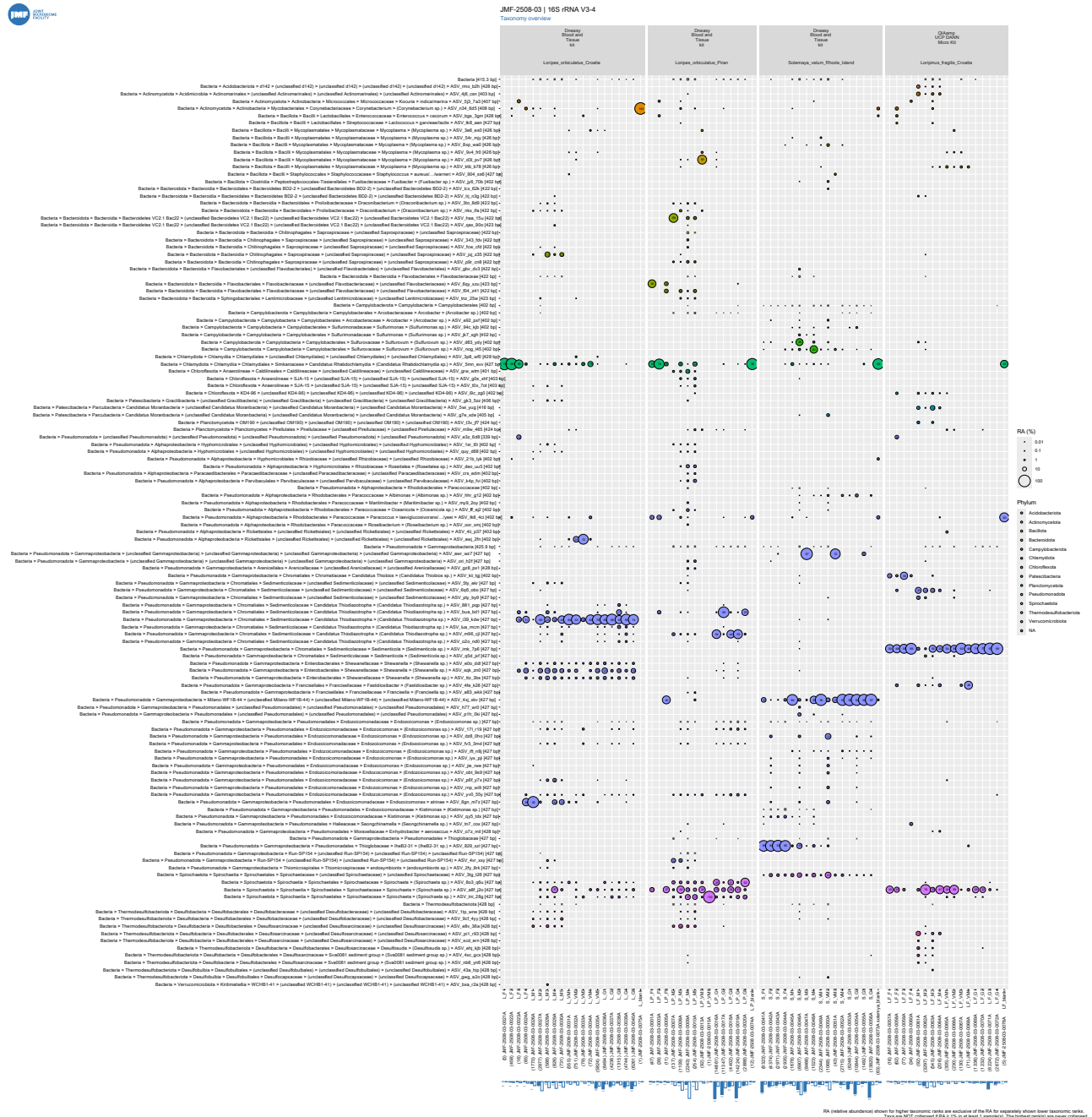

Supplementary Figure S1. Full bacterial community composition for sequencing batch JMF-2508-03 (V3-V4 dataset)
Species included: *Loripes orbiculatus* (Piran, Slovenia), *Loripes orbiculatus* (Rovinj, Croatia), *Loripinus fragilis, Solemya velum.* Supplementary Figure S1 presents the complete taxonomic composition of all bacterial ASVs detected in sequencing batch JMF-2508-03 based on relative abundance after quality filtering and contaminant removal. Unlike the main text, which summarises only the dominant symbiont lineages, this figure displays the full microbial community across all tissues and species, enabling direct comparison of low-abundance taxa and microbiome diversity within each host.

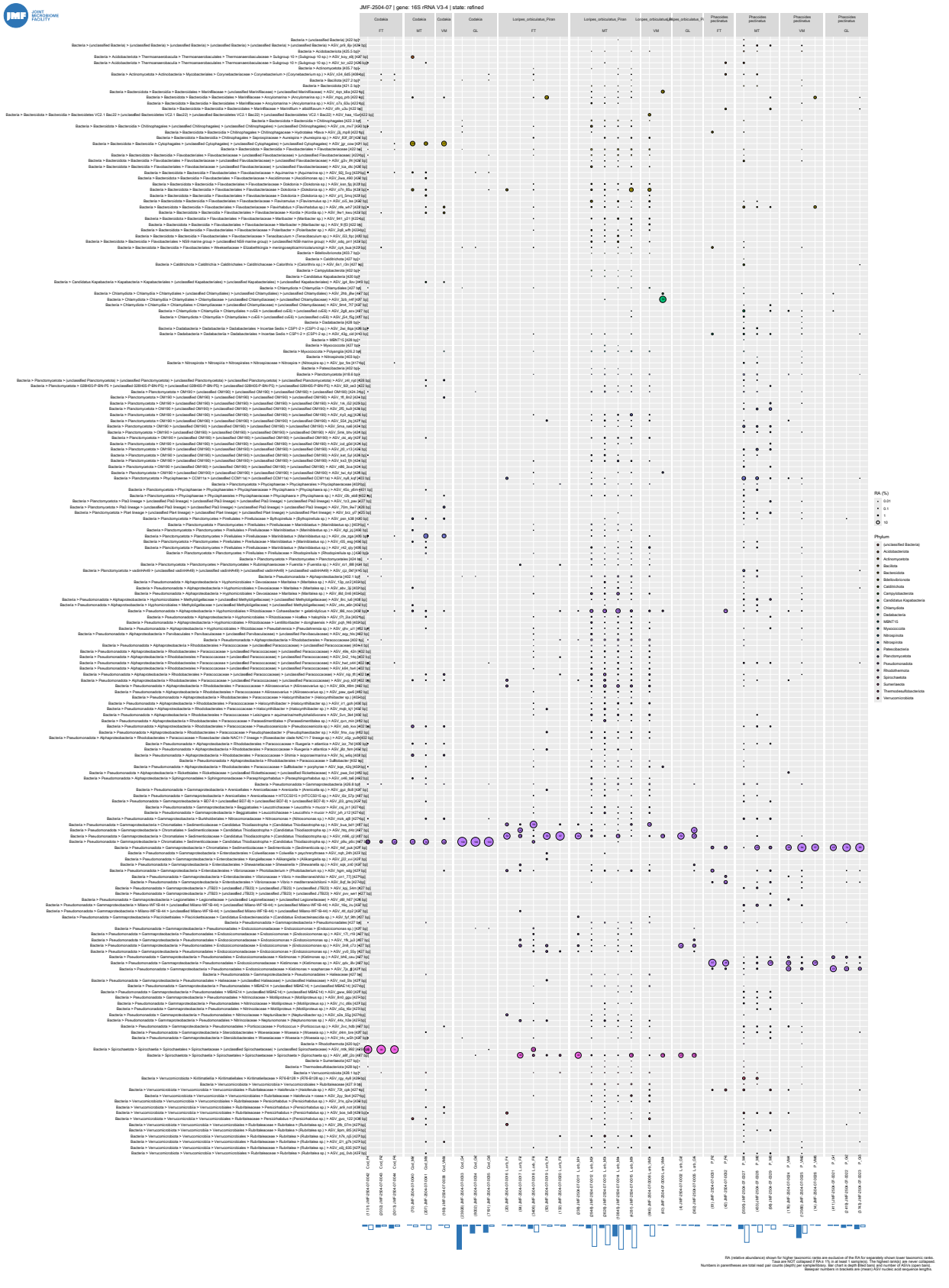

Supplementary Figure S2. Full bacterial community composition for sequencing batch JMF-2504-07 (V3-V4 dataset)
Species included: *Codakia orbicularis, Phacoides pectinatus, Loripes orbiculatus* (Piran, winter) — excluded from analyses but shown for completeness. Supplementary Figure S2 illustrates the full microbial community structure detected in sequencing batch JMF-2504-07, shown as relative abundance bar plots for every sample and tissue. This figure displays all bacterial ASVs represented in the dataset, including low-abundance and rare taxa, to provide transparency regarding the complete taxonomic landscape prior to focusing on the most abundant symbionts in the main text.

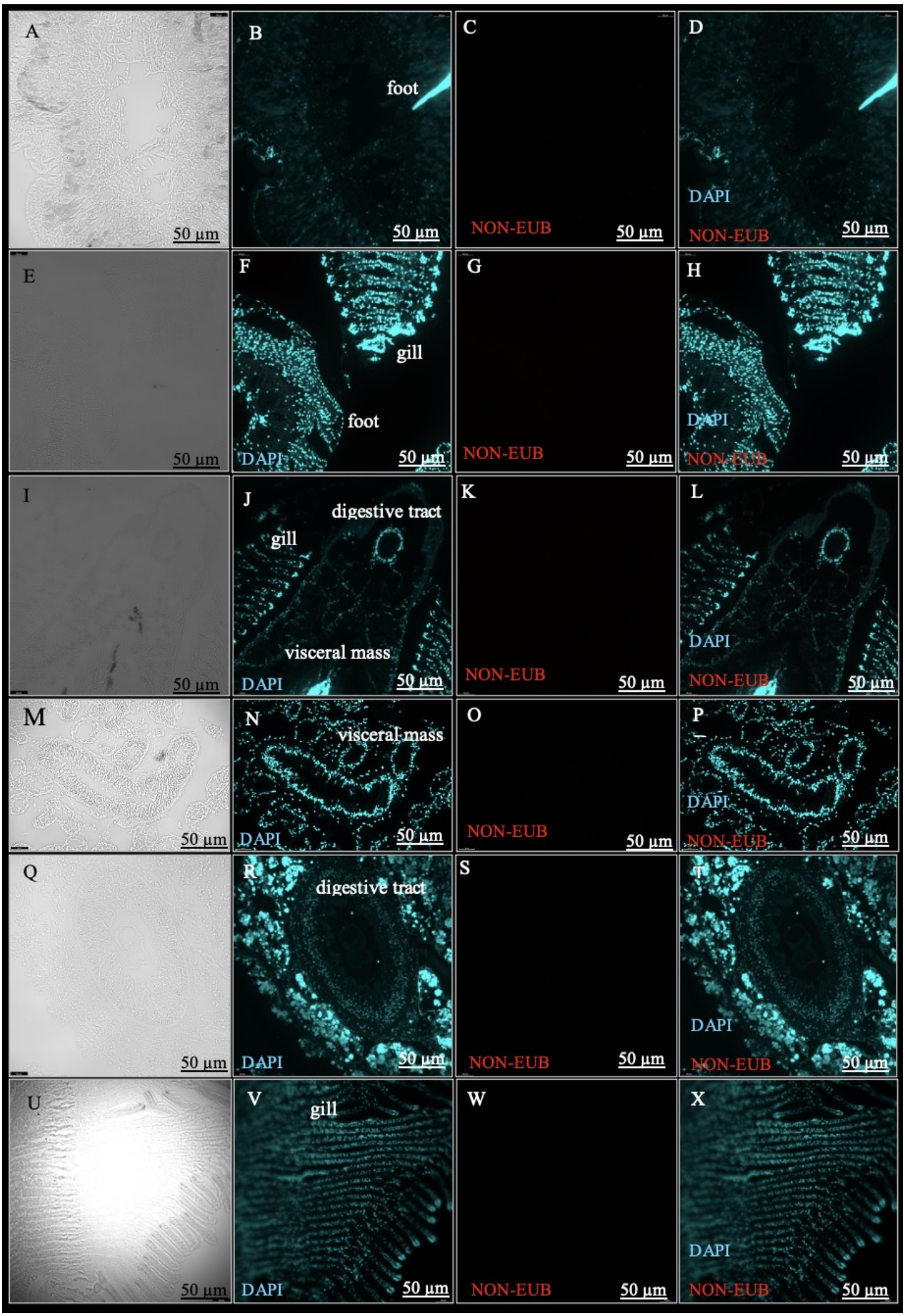
A
50 μm
B
foot
50 μm
C
NON-EUB
50 μm
D
DAPI
NON-EUB
50 μm
E
50 μm
F
gill
foot
DAPI
50 μm
G
NON-EUB
50 μm
H
DAPI
NON-EUB
50 μm
I
50 μm
J
digestive tract
gill
visceral mass
DAPI
50 μm
K
NON-EUB
50 μm
L
DAPI
NON-EUB
50 μm
M
50 μm
N
visceral mass
DAPI
50 μm
O
NON-EUB
50 μm
P
DAPI
NON-EUB
50 μm
Q
50 μm
R
digestive tract
DAPI
50 μm
S
NON-EUB
50 μm
T
DAPI
NON-EUB
50 μm
U
50 μm
V
gill
DAPI
50 μm
W
NON-EUB
50 μm
X
DAPI
NON-EUB
50 μm

Supplementary Figure S3. Fluorescence in situ hybridisation (FISH) of all non-EUB control images across species.

This figure presents the complete set of negative-control FISH images generated using the NON-EUB nonsense probe for all examined species: A-D) *Loripes orbiculatus* (Piran), E-H) *Loripes orbiculatus* (Rovinj), I-L) *Loripinus fragilis*, M-P) *Phacoides pectinatus*, Q-T) *Codakia orbicularis*, and U-X) *Solemya velum*. The NON-EUB probe was used to detect nonspecific hybridisation, tissue autofluorescence, or probe-related artefacts. Across species, NON-EUB images showed only diffuse background signal corresponding to intrinsic tissue autofluorescence, with no discrete punctate or cell-associated fluorescence. In all cases, the intensity and distribution of NON-EUB signal differed clearly from those obtained with symbiont-specific probes (Sym845, SymAf576, Sed642, and Svsym47). From left to right showing Bright-field, DAPI, NON-EUB, Merged.